SIAM J. SCI. COMPUT. © 2025 Society for Industrial and Applied Mathematics
Vol. 47, No. 3, pp. B710–B734

A NORMALIZED GRADIENT FLOW METHOD FOR COMPUTING GROUND STATES OF SPIN-2 BOSE–EINSTEIN CONDENSATES*

WEIZHU BAO†, QINGLIN TANG‡, AND YONGJUN YUAN§

Abstract. We propose and analyze an efficient and accurate numerical method for computing ground states of spin-2 Bose–Einstein condensates (BECs) by using the normalized gradient flow (NGF). In order to successfully extend the NGF to spin-2 BECs which have five components in the vector wave function but with only two physical constraints on total mass conservation and magnetization conservation, two important techniques are introduced for designing the proposed numerical method. The first one is to systematically investigate the ground state structure and property of spin-2 BECs within a spatially uniform system, which can be used for how to properly choose initial data in the NGF for computing ground states of spin-2 BECs. The second one is to introduce three additional projection conditions based on the relations between the chemical potentials, together with the two existing physical constraints, such that the five projection parameters used in the projection step of the NGF can be uniquely determined. Then a backward-forward Euler finite difference method is adapted to discretize the NGF. We prove rigorously that there exists a unique solution of the nonlinear system for determining the five projection parameters in the full discretization of the NGF under a mild condition on the time step size. Extensive numerical results on ground states of spin-2 BECs with different types of phases and under different potentials are reported to show the efficiency and accuracy of the proposed numerical method and to demonstrate several interesting physical phenomena on ground states of spin-2 BECs.

Key words. spin-2 Bose–Einstein condensate, Gross–Pitaevskii energy functional, ground state, normalized gradient flow, backward-forward Euler finite difference method

MSC codes. 35Q55, 49J45, 65N06, 65N12, 65Z05, 81-08

DOI. 10.1137/24M1667683

1. Introduction.

Since its experimental realization in 1995 [2, 17, 26], the Bose–Einstein condensate (BEC) has stimulated great excitement in the physical community and regained vast interests in atomic and molecular as well as condensed matter physics. At early stage, atoms were magnetically trapped in BEC experiments and hence their spin degrees of freedom were frozen [2, 17, 26]. Nevertheless, recently developed optical trapping techniques [36] have enabled one to release the spin internal degrees of freedom, opening up a new research arena of quantum many-body systems named spinor BEC [21, 27, 34]. Extensive theoretical and experimental studies have been carried out to reveal numerous new quantum phenomena which are generally absent in a spin-frozen condensate [16, 24, 28, 29, 30, 31, 39, 41, 42]. Within the

*Submitted to the journal's Software, High-Performance Computing, and Computational Science and Engineering section June 7, 2024; accepted for publication (in revised form) March 10, 2025; published electronically June 6, 2025.
https://doi.org/10.1137/24M1667683
Funding: This work was partially supported by the National Key R&D Program of China (grant 2024YFA1012803) and the Natural Science Foundation of Sichuan Province (Grant No. 2024NS-FSC0438) (Q. Tang), National Natural Science Foundation of China grants 11971335 (Q. Tang) and 12471375 (Y. Yuan), and the Ministry of Education of Singapore under its Academic Research Fund MOE-T2EP20122-0002 (A-8000962-00-00) (W. Bao).

†Department of Mathematics, National University of Singapore, Singapore 119076 (matbaowz@nus.edu.sg, https://blog.nus.edu.sg/matbwz/).
‡School of Mathematics, Sichuan University, Chengdu, 610064 People's Republic of China (qinglin_tang@scu.edu.cn, http://www.qinglin-tang-scu.com).
§Corresponding author. LCSM (MOE), School of Mathematics and Statistics, Hunan Normal University, Changsha, Hunan, 410081 People's Republic of China (yyj1983@hunnu.edu.cn).

mean-field approximation, in contrast with a spin-frozen BEC whose order parameter can be well described by a scalar wave function ϕ, a spin-F ($F \in \mathbb{N}$) BEC is described by a macroscopic complex-valued vector wave function Φ consisting of $2F+1$ components, each of which characterizes one of the $2F+1$ hyperfine states ($m_F = -F, \dots, F$). In this paper, we consider spin-2 BECs, i.e., $F = 2$.

One important problem in the theoretical study of a spin-2 BEC is to find its ground state so as to initialize its dynamics and to predict new important phases of the ground state which can be later compared with or confirmed by those physical experimental observations. The ground state of a spin-2 BEC is defined as the minimizer of the following dimensionless Gross–Pitaevskii (GP) energy functional [7, 29, 38]:

$$\mathcal{E}(\Phi) = \int_{\mathbb{R}^d} \left[\sum_{\ell=-2}^{2} \left(\frac{1}{2}|\nabla \phi_\ell|^2 + V(\boldsymbol{x})|\phi_\ell|^2 \right) + \frac{\beta_0}{2}\rho^2 + \frac{\beta_1}{2}|\mathbf{F}|^2 + \frac{\beta_2}{2}|A_{00}|^2 \right] d\boldsymbol{x}, \tag{1.1}$$

satisfying both the *mass* (1.2) and the *magnetization* (1.3) constraints:

$$\mathcal{N}(\Phi(\boldsymbol{x})) := \sum_{\ell=-2}^{2} \int_{\mathbb{R}^d} |\phi_\ell(\boldsymbol{x})|^2 d\boldsymbol{x} = 1, \tag{1.2}$$

$$\mathcal{M}(\Phi(\boldsymbol{x})) := \sum_{\ell=-2}^{2} \int_{\mathbb{R}^d} \ell |\phi_\ell(\boldsymbol{x})|^2 d\boldsymbol{x} = M. \tag{1.3}$$

Here, $M \in [-2, 2]$ is a given constant, $\boldsymbol{x} \in \mathbb{R}^d$ ($d = 1, 2, 3$) is the spatial variable, $\Phi(\boldsymbol{x}) =: \big(\phi_2(\boldsymbol{x}), \phi_1(\boldsymbol{x}), \phi_0(\boldsymbol{x}), \phi_{-1}(\boldsymbol{x}), \phi_{-2}(\boldsymbol{x})\big)^T$ is the wave function, $\rho := \sum_{\ell=-2}^{2} \rho_\ell$ is the total density with $\rho_\ell = |\phi_\ell(\boldsymbol{x})|^2$ being the ℓth component density, and β_0, β_1, β_2 are real constants characterizing the spin-independent interaction, spin-exchange interaction, and spin-singlet interaction, respectively. In addition, $V(\boldsymbol{x})$ is a real-valued function representing the external trapping potential, $A_{00}(\Phi) := \big(2\phi_2\phi_{-2} - 2\phi_1\phi_{-1} + \phi_0^2\big)/\sqrt{5}$ is the amplitude of the spin-singlet pair, $\mathbf{F}(\Phi) := [F_x(\Phi), F_y(\Phi), F_z(\Phi)]^\top$ is the spin vector, and its components are defined as [7]:

$$\begin{aligned} &F_x = \mathrm{Re}(F_+),\ F_y = \mathrm{Im}(F_+),\ \text{with } F_+ = 2\big(\bar{\phi}_2\phi_1 + \bar{\phi}_{-1}\phi_{-2}\big) + \sqrt{6}\big(\bar{\phi}_1\phi_0 + \bar{\phi}_0\phi_{-1}\big), \\ &F_z = 2\big(|\phi_2|^2 - |\phi_{-2}|^2\big) + |\phi_1|^2 - |\phi_{-1}|^2, \end{aligned}$$

where $\bar{f}$ denotes the complex conjugate of f. The ground state $\Phi_g(\boldsymbol{x})$ is the solution of the following nonconvex minimization problem:

$$\Phi_g := \arg\min_{\Phi \in \mathbb{S}} \mathcal{E}(\Phi), \tag{1.4}$$

where the nonconvex set $\mathbb{S}$ is defined as

$$\mathbb{S} = \left\{ \Phi = (\phi_2, \phi_1, \phi_0, \phi_{-1}, \phi_{-2})^T \in \mathbb{C}^5 \mid \mathcal{N}(\Phi) = 1,\ \mathcal{M}(\Phi) = M,\ \mathcal{E}(\Phi) < \infty \right\}. \tag{1.5}$$

Existence and uniqueness of the ground state (1.4) was carried out in [7, 29, 30]. Meanwhile, validity of the so-called single mode approximation (SMA) of the ground state (which simplifies the ground state computation) is partially investigated. Different numerical methods have been proposed to compute the ground state of a scalar BEC [1, 3, 4, 5, 8, 9, 11, 14, 15, 19, 20, 22, 23, 25, 40] and a spin-1 BEC [10, 13, 15, 18, 33, 43, 44, 45]. Among them, a simple and most popular method is the normalized gradient flow (NGF) (or imaginary time method) incorporated with a proper discretization scheme to evolve the resulted gradient flow under normalization of the wave function [5, 11, 13, 15]. However, to extend the NGF from single-component BEC and spin-1 BEC to spin-2 BEC, due to the fact that we only have two conservation conditions (1.2) and (1.3) and there are five projection constants to be determined in the projection step, it is unclear whether the NGF method could be easily and straightforwardly extended to compute ground states of spin-2 BECs. A projection gradient method [38] was proposed to compute ground states of spin-2 BECs, where a continuous normalized gradient flow (CNGF) was discretized by the Crank–Nicolson finite difference method with a proper and special way to deal with the nonlinear terms. This scheme was proved to be energy-diminishing and to conserve both the total mass and magnetization in the discrete level. However, a fully nonlinear coupled system needs to be solved at each time step, which introduces much computational cost, especially in three dimensions. Recently, numerical methods were presented for computing ground states of spin-2 BECs based on the NGF with inaccurate projections [18, 37]. The main objective of this paper is to present and analyze a numerical method for computing ground states of spin-2 BECs via the NGF. In order to do so, two main techniques are presented, which are (i) to carry out a systematic study on the ground state structure and property of a spin-2 BEC within a spatially uniform system, which is then used to choose simple and proper initial data in the NGF for computing ground states of spin-2 BECs, and (ii) to introduce three additional projection conditions based on the relations between the chemical potentials of a spin-2 BEC for overcoming the fact that there are five components in the vector wave function but with only two constraints on total mass conservation and total magnetization conservation. In fact, the proposed three additional projection conditions, together with total mass conservation and magnetization conservation, can completely determine the five projection constants used in projection step of the NGF. This enables us to extend the simple and powerful NGF method to compute ground states of spin-2 BECs.

The rest of the paper is organized as follows. In section 2, ground state structure and property of spin-2 BEC in a spatially uniform system are investigated systematically. In section 3, a NGF is constructed by introducing three additional projection conditions and then a backward-forward Euler finite difference method is presented to discretize the NGF. In section 4, we report extensive numerical results on ground states of spin-2 BECs with different types of phases and under different potentials in one and two dimensions. Finally, some conclusions are drawn in section 5.

2. Ground states and their properties.

In this section, we mainly investigate the ground state structure and property of a spin-2 BEC.

2.1. Euler–Lagrange equations and classification of ground states.

The Euler–Lagrange equation associated to the minimization problem (1.4) reads as

$$
\begin{cases}
(\mu \pm 2\lambda)\phi_{\pm 2} = (H_\rho \pm 2\beta_1 F_z)\,\phi_{\pm 2} + \beta_1 F_\mp \phi_{\pm 1} + \dfrac{\beta_2}{\sqrt{5}} A_{00}\bar{\phi}_{\mp 2}, \\
(\mu \pm \lambda)\phi_{\pm 1} = (H_\rho \pm \beta_1 F_z)\,\phi_{\pm 1} + \beta_1 \left(\dfrac{\sqrt{6}}{2} F_\mp \phi_0 + F_\pm \phi_{\pm 2}\right) - \dfrac{\beta_2}{\sqrt{5}} A_{00}\bar{\phi}_{\mp 1}, \\
\mu\phi_0 = H_\rho \phi_0 + \dfrac{\sqrt{6}}{2}\beta_1\big(F_+\phi_1 + F_-\phi_{-1}\big) + \dfrac{\beta_2}{\sqrt{5}} A_{00}\bar{\phi}_0.
\end{cases}
\tag{2.1}
$$

Here, $H_\rho = -\nabla^2/2 + V(\boldsymbol{x}) + \beta_0\rho$, $F_- = \bar{F}_+$, and μ and λ are Lagrange multipliers associated to the mass and magnetization constraints (1.2)–(1.3). Thus the ground state of (1.4) can also be viewed as the eigenfunction of the nonlinear eigenvalue problem (2.1) with constraints (1.2)–(1.3), which has the lowest energy among all eigenfunctions. Other eigenfunctions with higher energy are called excited states.

As carried out in [7], the ground state of (1.4) is unique up to a phase-rotation; i.e., $\Phi_g^1 := (\phi_2^{1,g}, \phi_1^{1,g}, \phi_0^{1,g}, \phi_{-1}^{1,g}, \phi_{-2}^{1,g})^T$ and $\Phi_g^2 := (\phi_2^{2,g}, \phi_1^{2,g}, \phi_0^{2,g}, \phi_{-1}^{2,g}, \phi_{-2}^{2,g})^T$ are regarded as the same if there exists a constant vector $\boldsymbol{\alpha} := (\alpha_2, \alpha_1, \alpha_0, \alpha_{-1}, \alpha_{-2})^T = \big(e^{i(2\theta_1-\theta_0)}, e^{i\theta_1}, e^{i\theta_0}, e^{i(2\theta_0-\theta_1)}, e^{i(3\theta_0-2\theta_1)}\big)^T$ with $\theta_0, \theta_1 \in \mathbb{R}$ such that $\phi_\ell^{1,g} = \alpha_\ell \phi_\ell^{2,g}$ for $\ell = -2, \ldots, 2$. According to [24, 29], the phase of the ground state Φ_g of (1.4) can be classified into three categories based on the values of $|F_+(\Phi_g)|$ and $|A_{00}(\Phi_g)|$: (i) the ferromagnetic phase if $|F_+(\Phi_g)| > 0$ and $A_{00}(\Phi_g) = 0$, (ii) the nematic phase if $F_+(\Phi_g) = 0$ and $|A_{00}(\Phi_g)| > 0$, and (iii) the cyclic phase if $F_+(\Phi_g) = A_{00}(\Phi_g) = 0$. When $M = 2$ or -2, the constraints (1.2)–(1.3) only allow one component, i.e., ϕ_2 or ϕ_{-2}, to be nonzero. Therefore, (1.4) can be reduced to compute the ground state of a single component BEC with ϕ_2 or ϕ_{-2}, which has been well studied [9, 11, 12, 14]. In addition, if one replaces the magnetization $\mathcal{M}(\Phi) = M$ in (1.5) by $\mathcal{M}(\Phi) = -M$, it is easy to see that the ground state $\Phi_g := (\phi_2^g, \phi_1^g, \phi_0^g, \phi_{-1}^g, \phi_{-2}^g)^T$ of (1.4) can be simply replaced by $\tilde{\Phi}_g := (\phi_{-2}^g, \phi_{-1}^g, \phi_0^g, \phi_1^g, \phi_2^g)^T$. Thus, for simplicity of notations and presentation, from now on, we only consider the magnetization $M \in [0, 2)$.

Remark 2.1. In the literature [7, 29], instead of the ground state being defined as the minimizer of the energy function $\mathcal{E}(\Phi)$ under two constraints of the total mass conservation $\mathcal{N}(\Phi) = 1$ and total magnetization $\mathcal{M}(\Phi) = M$ with $M \in [-2, 2]$, i.e., (1.4), another type of ground state has also been studied. It is defined as the minimizer of energy function $\mathcal{E}(\Phi)$ under only the mass constraint (1.2), i.e.,

$$\tilde{\Phi}_g := \arg \min_{\|\Phi\|=1} \mathcal{E}(\Phi). \tag{2.2}$$

In fact, the above minimization problem can be obtained via the minimization problem (1.4) by further minimizing for $M \in [-2, 2]$, i.e.,

$$\tilde{\Phi}_g := \arg \min_{M \in [-2,2]} \Phi_g^M, \quad \text{with} \quad \Phi_g^M := \arg \min_{\Phi \in \mathbb{S}} \mathcal{E}(\Phi). \tag{2.3}$$

The Euler–Lagrange equation associated to the minimization problem (2.2) is given by

$$\begin{cases} \mu\phi_{\pm 2} = (H_\rho + \beta_0\rho \pm 2\beta_1 F_z)\,\phi_{\pm 2} + \beta_1 F_\mp \phi_{\pm 1} + \dfrac{\beta_2}{\sqrt{5}} A_{00} \bar{\phi}_{\mp 2}, \\ \mu\phi_{\pm 1} = (H_\rho + \beta_0\rho \pm \beta_1 F_z)\,\phi_{\pm 1} + \beta_1 \left(\dfrac{\sqrt{6}}{2} F_\mp \phi_0 + F_\pm \phi_{\pm 2}\right) - \dfrac{\beta_2}{\sqrt{5}} A_{00} \bar{\phi}_{\mp 1}, \\ \mu\phi_0 = (H_\rho + \beta_0\rho)\,\phi_0 + \dfrac{\sqrt{6}}{2}\beta_1 \big(F_+\phi_1 + F_-\phi_{-1}\big) + \dfrac{\beta_2}{\sqrt{5}} A_{00} \bar{\phi}_0, \end{cases} \tag{2.4}$$

where μ is the Lagrange multiplier associated to the mass constraint (1.2).

2.2. Ground states in a spatially uniform system. In this section, we consider a spin-2 BEC in a spatially uniform system, i.e., the GP functional (1.1) without potential (i.e., $V(\boldsymbol{x}) \equiv 0$) on a bounded domain $\mathcal{D}$ with measure $|\mathcal{D}| = 1$ and periodic boundary condition. This will be applied directly in section 2.3 to construct the so-called single mode approximation (SMA) of the ground states in a spatial nonuniform system, which will reduce significantly the difficulty and computational cost to obtain a ground state of spin-2 BECs. In addition, in the parameter region where SMA is invalid, the ground states carried out here can help build more efficient initial data for the algorithm proposed in section 3.2 to accelerate its convergence.

In a spatially uniform system, all ground states are constants in form of [29]

$$\Phi(\boldsymbol{x}) \equiv \boldsymbol{\xi} := (\xi_2, \xi_1, \xi_0, \xi_{-1}, \xi_{-2})^T, \quad \boldsymbol{x} \in \overline{\mathcal{D}}, \tag{2.5}$$

where $\xi_j \in \mathbb{C}$ for $j = -2, -1, 0, 1, 2$. Plugging (2.5) into (1.1) with $V(\boldsymbol{x}) \equiv 0$ and $\Phi(\boldsymbol{x}) = \boldsymbol{\xi}$ and replacing $\mathbb{R}^d$ by $\mathcal{D}$, after a detailed computation, we obtain

$$\mathcal{E}(\Phi) = \mathcal{E}_U(\boldsymbol{\xi}) := \frac{1}{2}\left[\left(\beta_1|\tau|^2 + \frac{\beta_2}{5}|\delta|^2\right) + \left(\beta_0 + \beta_1 M^2\right)\right] =: E\,(\tau, \delta)\,, \tag{2.6}$$

where

$$\begin{cases} \tau := \tau(\boldsymbol{\xi}) = F_+(\boldsymbol{\xi}) = 2\big(\bar{\xi}_2\xi_1 + \bar{\xi}_{-1}\xi_{-2}\big) + \sqrt{6}\big(\bar{\xi}_1\xi_0 + \bar{\xi}_0\xi_{-1}\big), \\ \delta := \delta(\boldsymbol{\xi}) = A_{00}(\boldsymbol{\xi}) = 2\xi_2\xi_{-2} - 2\xi_1\xi_{-1} + \xi_0^2. \end{cases} \tag{2.7}$$

Actually, τ and δ are precisely the quantities which will be used later to characterize ground states as either ferromagnetic, nematic, or cyclic. The conservation of *mass* (1.2) and *magnetization* (1.3) leads to

$$\begin{cases} |\xi_2|^2 + |\xi_{-2}|^2 + |\xi_0|^2 + |\xi_1|^2 + |\xi_{-1}|^2 = 1, \\ 2(|\xi_2|^2 - |\xi_{-2}|^2) + |\xi_1|^2 - |\xi_{-1}|^2 = M \end{cases} \tag{2.8}$$

for given $M \in [0, 2)$. Solving (1.4)–(1.5) for ground state $\Phi_g(\boldsymbol{x})$ is now equivalent to solving the following minimization problem for minimizer $\boldsymbol{\xi}_g := (\xi_2^g, \xi_1^g, \xi_0^g, \xi_{-1}^g, \xi_{-2}^g)^T$ as

$$\boldsymbol{\xi}_g := \arg\min_{\boldsymbol{\xi} \in \mathbb{S}_C} \mathcal{E}_U(\boldsymbol{\xi}), \quad \mathbb{S}_C = \left\{ \boldsymbol{\xi} \in \mathbb{C}^5 \;\middle|\; \sum_{\ell=-2}^{2} |\xi_\ell|^2 = 1,\ \sum_{\ell=-2}^{2} \ell|\xi_\ell|^2 = M \right\}. \tag{2.9}$$

In the following, we show that the minimization problem (2.9) on complex manifold $\mathbb{S}_C$ can be reduced to a minimization problem on the real manifold $\mathbb{S}_R = \mathbb{S}_C \cap \mathbb{R}^5$.

LEMMA 2.1. *If $\boldsymbol{\xi} \in \mathbb{R}^5$, then the system* (2.8) *has a real solution if and only if*

$$\tau^2(\boldsymbol{\xi}) + 4\,\delta^2(\boldsymbol{\xi}) \le 4 - M^2. \tag{2.10}$$

Proof. First, we prove the necessary condition; i.e., we assume $\boldsymbol{\xi} \in \mathbb{R}^5$ and the system (2.8) has a real solution. By (2.7) and (2.8), we have

$$(\xi_2 - \xi_{-2})^2 + (\xi_1 + \xi_{-1})^2 = 1 - \delta. \tag{2.11}$$

Noticing $|\delta| \le \sum_{\ell=-2}^{2} \xi_\ell^2 = 1$ and denoting $p = \sqrt{1-\delta} \ge 0$, then there exists a constant $\theta \in [0, 2\pi)$ such that

$$\begin{cases} \xi_{-2} - \xi_2 = p\cos\theta, \\ \xi_1 + \xi_{-1} = p\sin\theta, \end{cases} \iff \begin{cases} \xi_{-2} = p\cos\theta + \xi_2, \\ \xi_{-1} = p\sin\theta - \xi_1. \end{cases} \tag{2.12}$$

We then prove (2.10) is valid by considering four different parameter cases. To simplify the presentation, in the following, we only state the formula for ξ_0, ξ_1, and ξ_2, and the expressions of ξ_{-1} and ξ_{-2} can be obtained directly from (2.12).

Case (i). If $\delta = 1$, then $p = 0$. From (2.12), we obtain $\xi_2 = \xi_{-2}$ and $\xi_1 = -\xi_{-1}$. By (2.8) and (2.7), we have

$$M = \tau = 0, \quad \Longrightarrow \quad \tau^2 + 4\delta^2 \le 4 - M^2.$$

Case (ii). If $\delta<1$ (and thus $p>0$) and $\cos\theta=0$, then $\xi_{-2}=\xi_2$ and $\xi_{-1}=p-\xi_1$. Plugging them into (2.7) and (2.8), by a simple calculation, we obtain

$$\xi_0=(\tau-2p\xi_2)/(p\sqrt{6}), \tag{2.13}$$
$$2|\xi_2|^2+|\xi_0|^2+(M+p^2)^2/(2p^2)=1+M. \tag{2.14}$$

Thereby, combining (2.13) and (2.14), we have

$$16p^2\xi_2^2-4p\tau\xi_2+3p^4-6p^2+3M^2+\tau^2=0. \tag{2.15}$$

Note that (2.15) has a real solution if and only if the corresponding discriminant

$$\Delta:=-48p^2(4\delta^2+\tau^2+4M^2-4)\geq 0, \tag{2.16}$$

which immediately implies

$$\tau^2+4\delta^2\leq 4-4M^2\leq 4-M^2. \tag{2.17}$$

Case (iii). If $\delta<1$ (and thus $p>0$) and $\sin\theta=0$. Similarly, we obtain

$$\xi_2=\frac{(2p^2+M)\cos\theta}{4p},\quad \xi_1=\frac{\tau\cos\theta}{2p},\quad \xi_0^2=\frac{4-M^2-4\delta^2-4\tau^2}{8p^2}. \tag{2.18}$$

Thus ξ_0 is real if and only if $4-M^2-4\delta^2-4\tau^2\geq 0$, which again implies

$$\tau^2+4\delta^2\leq 4-M^2-3\tau^2\leq 4-M^2.$$

Case (iv). If $\delta<1$ and $\sin(2\theta)\neq 0$. Plugging (2.12) into (2.8), we have

$$\xi_2=-(M+2p^2-p^2\sin^2\theta-2p\sin\theta\xi_1)/(4p\cos\theta), \tag{2.19}$$
$$\xi_0=\frac{4-6\sin^2\theta}{\sqrt{6}\sin(2\theta)}\xi_1+\frac{M-2p^2+3p^2\sin^2\theta}{2\sqrt{6}p\cos\theta}+\frac{\tau}{\sqrt{6}p\sin\theta}, \tag{2.20}$$
$$A\xi_1^2+B\xi_1+C=0, \tag{2.21}$$

with

$$\begin{aligned}
A&=8\csc^2(2\theta),\\
B&=\frac{\csc^2\theta\sec^2\theta}{4p}\Big[5\tau\cos\theta+3\tau\cos(3\theta)-5M\sin\theta-8p^2\sin\theta+3M\sin(3\theta)\Big],\\
C&=\frac{1}{2p^2}\Bigg[\tau^2\csc^2\theta+(M-2p^2)\tau\csc\theta\sec\theta-\frac{1}{2}\sec^2\theta\big(-2M^2+6\delta p^2-Mp^2+p^4\\
&\qquad+3p^2(2\delta+M+p^2)\cos(2\theta)-3p^2\tau\sin(2\theta)\big)\Bigg].
\end{aligned}$$

Similarly, (2.21) has a real solution if and only if the corresponding discriminant

$$\Delta=-\frac{3\csc^2\theta\sec^2\theta}{p^2}\Big[3(M\sin\theta+\tau\cos\theta)^2+4\delta^2+\tau^2+M^2-4\Big]\geq 0, \tag{2.22}$$

which implies

$$4-M^2-(4\delta^2+\tau^2)\geq 3(M\sin\theta+\tau\cos\theta)^2\geq 0\quad\Longrightarrow\quad \tau^2+4\delta^2\leq 4-M^2.$$

Second, we prove the sufficient condition; i.e., we assume (2.10) is valid. When $\delta=1$, then $M=\tau=0$, and thus $\xi=(0,0,1,0,0)^T$ is a real solution of (2.8); when $\delta<1$ and $M=0$, then (2.16) is satisfied, and thus (2.13)–(2.15) is a real solution; and when $\delta<1$ and $M\neq 0$, by choosing $\theta=\pi-\arctan(\tau/M)$ such that $M\sin\theta=-\tau\cos\theta$ and (2.22) is fulfilled, then (2.19)–(2.21) is a real solution. ∎

LEMMA 2.2. *For all* $\boldsymbol{\xi} \in \mathbb{S}_C$*, we have*

$$|\tau(\boldsymbol{\xi})|^2 + 4\,|\delta(\boldsymbol{\xi})|^2 \leq 4 - M^2, \tag{2.23}$$

and there exists a $\boldsymbol{\zeta}_R \in \mathbb{S}_R$ *such that* $\mathcal{E}_U(\boldsymbol{\zeta}_R) = \mathcal{E}_U(\boldsymbol{\xi})$*. Therefore, the minimization problem* (2.9) *has at least a real ground state.*

Proof. We prove this lemma by considering two different cases.

Case (i). If $\delta(\boldsymbol{\xi}) = 0$, noticing that

$$\boldsymbol{\xi} \in \mathbb{S}_C \qquad \Longrightarrow \qquad \boldsymbol{\zeta} := (|\xi_2|, |\xi_1|, |\xi_0|, |\xi_{-1}|, |\xi_{-2}|)^T \in \mathbb{S}_R,$$

and hence the system (2.8) is fulfilled for $\boldsymbol{\zeta}$. By Lemma 2.1, we have

$$|\tau(\boldsymbol{\xi})|^2 + 4|\delta(\boldsymbol{\xi})|^2 = |\tau(\boldsymbol{\xi})|^2 \leq \tau^2(\boldsymbol{\zeta}) \leq \tau^2(\boldsymbol{\zeta}) + 4\delta^2(\boldsymbol{\zeta}) \leq 4 - M^2.$$

Case (ii). If $\delta(\boldsymbol{\xi}) \neq 0$, noticing that

$$\begin{aligned} \max_{\boldsymbol{\xi}\in\mathbb{S}_C} \left\{|\tau(\boldsymbol{\xi})|^2 + 4|\delta(\boldsymbol{\xi})|^2 + M^2\right\} &= \max_{\boldsymbol{\xi}\in\mathbb{S}_C} \left\{|\tau(\boldsymbol{\xi})|^2 + 4|\delta(\boldsymbol{\xi})|^2 + F_z^2(\boldsymbol{\xi})\right\} \\ &\leq \max_{\boldsymbol{\zeta}\in\mathbb{S}_1} \left\{|\tau(\boldsymbol{\zeta})|^2 + 4|\delta(\boldsymbol{\zeta})|^2 + F_z^2(\boldsymbol{\zeta})\right\}, \end{aligned} \tag{2.24}$$

with $\mathbb{S}_1 = \{\boldsymbol{\zeta} \in \mathbb{C}^5 \mid \sum_{\ell=-2}^{2} |\zeta_l|^2 = 1\}$; thus, to prove (2.23), we only need to show

$$\max_{\boldsymbol{\zeta}\in\mathbb{S}_1} \left\{|\tau(\boldsymbol{\zeta})|^2 + 4|\delta(\boldsymbol{\zeta})|^2 + F_z^2(\boldsymbol{\zeta})\right\} \leq 4. \tag{2.25}$$

Consider an auxiliary minimization problem

$$\boldsymbol{\zeta}_g := (\zeta_2^g, \zeta_1^g, \zeta_0^g, \zeta_{-1}^g, \zeta_{-2}^g)^T = \arg\min_{\boldsymbol{\zeta}\in\mathbb{S}_1} \mathcal{F}(\boldsymbol{\zeta}), \tag{2.26}$$

where the auxiliary functional $\mathcal{F}(\boldsymbol{\zeta})$ is defined as

$$\mathcal{F}(\boldsymbol{\zeta}) = -\left[|\tau(\boldsymbol{\zeta})|^2 + 4|\delta(\boldsymbol{\zeta})|^2 + F_z^2(\boldsymbol{\zeta})\right]. \tag{2.27}$$

It is clear that

$$\mathcal{F}(\boldsymbol{\zeta}_g) = -\max_{\boldsymbol{\zeta}\in\mathbb{S}_1} \left\{|\tau(\boldsymbol{\zeta})|^2 + 4|\delta(\boldsymbol{\zeta})|^2 + F_z^2(\boldsymbol{\zeta})\right\}, \tag{2.28}$$

and $\boldsymbol{\zeta}_g$ satisfies the Euler–Lagrange equation $\nabla_{\bar{\boldsymbol{\zeta}}} \mathcal{F}(\boldsymbol{\zeta}) = \lambda_{\boldsymbol{\zeta}}\, \boldsymbol{\zeta}$ with $\lambda_{\boldsymbol{\zeta}} \in \mathbb{R}$ being the Lagrange multiplier and $\bar{\boldsymbol{\zeta}}$ being the complex conjugate of $\boldsymbol{\zeta}$, i.e., $\nabla_{\bar{\boldsymbol{\zeta}}} \mathcal{F}(\boldsymbol{\zeta}_g) = \lambda_{\boldsymbol{\zeta}_g} \boldsymbol{\zeta}_g$. Hence, by denoting $\boldsymbol{\eta}_g = (\zeta_{-2}^g, -\zeta_{-1}^g, \zeta_0^g, -\zeta_1^g, \zeta_2^g)^T$, we have

$$\begin{cases} \bar{\boldsymbol{\zeta}}_g \cdot \nabla_{\bar{\boldsymbol{\zeta}}} \mathcal{F}(\boldsymbol{\zeta}_g) = \lambda_{\boldsymbol{\zeta}_g}, \\ \boldsymbol{\eta}_g \cdot \nabla_{\bar{\boldsymbol{\zeta}}} \mathcal{F}(\boldsymbol{\zeta}_g) = \lambda_{\boldsymbol{\zeta}_g} \boldsymbol{\eta}_g \cdot \boldsymbol{\zeta}_g, \end{cases} \quad \Longrightarrow \quad \begin{cases} -2(|\tau|^2 + 4|\delta|^2 + F_z^2) = \lambda_{\boldsymbol{\zeta}_g}, \\ (\lambda_{\boldsymbol{\zeta}_g} + 8)\delta = 0, \end{cases} \tag{2.29}$$

which leads to

$$\begin{cases} \lambda_{\boldsymbol{\zeta}_g} = -8, \\ |\tau(\boldsymbol{\zeta}_g)|^2 + 4|\delta(\boldsymbol{\zeta}_g)|^2 + F_z^2(\boldsymbol{\zeta}_g) = 4, \end{cases} \quad \Longrightarrow \quad \mathcal{F}(\boldsymbol{\zeta}_g) = -4. \tag{2.30}$$

Noticing (2.28), one gets (2.25). This, together with (2.24), concludes the desired inequality (2.23). Therefore, for all $\boldsymbol{\xi} \in \mathbb{S}_C$, let $\tau(\boldsymbol{\zeta}_R) = |\tau(\boldsymbol{\xi})|$ and $\delta(\boldsymbol{\zeta}_R) = |\delta(\boldsymbol{\xi})|$, and we have

$$\tau^2(\boldsymbol{\zeta}_R) + 4\delta^2(\boldsymbol{\zeta}_R) \leq 4 - M^2.$$

According to Lemma 2.1, the system (2.8) has a real solution $\boldsymbol{\zeta}_R \in \mathbb{S}_R$, which satisfies $\mathcal{E}_U(\boldsymbol{\zeta}_R) = \mathcal{E}_U(\boldsymbol{\xi})$. One immediately obtains

$$\min_{\boldsymbol{\xi}\in\mathbb{S}_C} \mathcal{E}_U(\boldsymbol{\xi}) = \min_{\boldsymbol{\zeta}_R\in\mathbb{S}_R} \mathcal{E}_U(\boldsymbol{\zeta}_R) = \min_{S_{\tau,\delta}} E(\tau,\delta) = \frac{1}{2}(\beta_0+\beta_1 M^2) + \frac{1}{2}\min_{S_{\tau,\delta}} f(\tau,\delta), \tag{2.31}$$

where

$$f(\tau,\delta) = \beta_1\tau^2 + \frac{\beta_2}{5}\delta^2 \quad \text{and} \quad S_{\tau,\delta} := \left\{\tau\in\mathbb{R},\ \delta\in\mathbb{R},\ \tau^2+4\delta^2 \le 4-M^2\right\}. \tag{2.32}$$

Obviously, for any given β_1 and β_2, the quadratic minimization problem

$$(\tau_g,\delta_g) := \arg\min_{S_{\tau,\delta}} f(\tau,\delta) \tag{2.33}$$

possesses at least a solution over the elliptic domain $S_{\tau,\delta}$. As a result, the minimization problem (2.9) has at least a real ground state. ∎

Thanks to Lemmas 2.1–2.2, noticing (2.6), to find the ground state $\boldsymbol{\xi}_g$ of (2.9) is then reduced to finding minimizers of the minimization problem (2.33). Actually, it can be solved analytically since it sets out to find minimizers of a quadratic function over an elliptic domain. To illustrate this, Figure 2.1 shows contour plots of the energy $E(\tau,\delta)$ for $\beta_0 = M = 0$ with different β_1 and β_2 on the elliptic domain $S_{\tau,\delta}$. From the figure, one can obtain the minimizers (τ_g,δ_g).

Noticing that if $\boldsymbol{\xi}$ solves (2.7)–(2.8) with τ, then $\tilde{\boldsymbol{\xi}} = (\xi_2, -\xi_1, \xi_0, -\xi_{-1}, \xi_{-2})^T$ solves (2.7)–(2.8) with the parameter $-\tau$. Thus it suffices to assume $\tau \ge 0$ for simplicity hereafter. To solve out analytically the minimization problem (2.33) on the elliptic domain $S_{\tau,\delta}$, we adapt the following elliptic-polar coordinates as

$$\tau = r\cos\theta, \quad \delta = \frac{1}{2} r\sin\theta, \quad \theta \in \left[-\frac{\pi}{2}, \frac{\pi}{2}\right), \quad r \in \left[0, \sqrt{4-M^2}\,\right], \tag{2.34}$$

in whose coordinate the function $f(\tau,\delta)$ (2.32) reads as follows:

$$\begin{aligned} f(\tau,\delta) &= \beta_1\tau^2 + \frac{\beta_2}{5}\delta^2 = \beta_1 r^2\cos^2\theta + \frac{\beta_2}{20} r^2 \sin^2\theta = \frac{\beta_2}{20} r^2 + \left(\beta_1 - \frac{\beta_2}{20}\right) r^2\cos^2\theta \\ &= \beta_1 r^2 + \left(\frac{\beta_2}{20} - \beta_1\right) r^2 \sin^2\theta, \qquad \theta \in \left[-\frac{\pi}{2}, \frac{\pi}{2}\right), \quad r \in \left[0, \sqrt{4-M^2}\,\right]. \end{aligned}$$

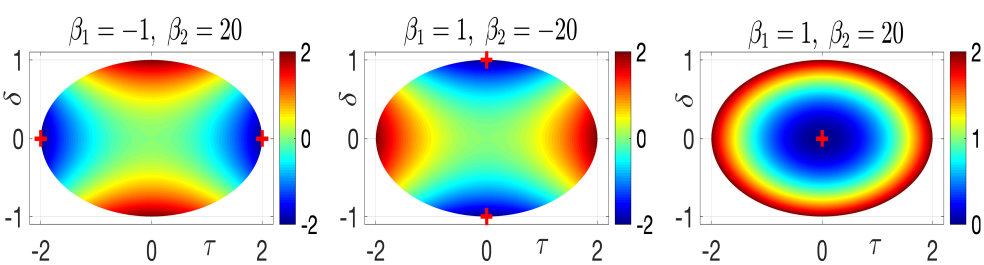

FIG. 2.1. *Contour plots of the energy $E(\tau,\delta)$ in (2.31) for $\beta_0 = M = 0$ with different $\beta_1 = -1$ and $\beta_2 = 20$ (left), $\beta_1 = 1$ and $\beta_2 = -20$ (middle), and $\beta_1 = 1$ and $\beta_2 = 20$ (right). "+" denote those points where the minimum values of $E(\tau,\delta)$ are achieved. According to the value (and position on the graph) of those points "+", one can immediately conclude that the phases of the corresponding ground state are in ferromagnetic (left), nematic (middle), and cyclic (right).*

Therefore, it is easy to obtain the following: (i) when $\beta_1<0$ and $\beta_2>20\beta_1$, from the last equality, $f(\tau,\delta)$ attains its minimum when $\sin^2\theta=0$ and $r=\sqrt{4-M^2}$, i.e., at $(\tau_g,\delta_g)=(\sqrt{4-M^2},0)$; (ii) when $\beta_2<0$ and $\beta_2<20\beta_1$, from the third equality, $f(\tau,\delta)$ attains its minimum when $\cos^2\theta=0$ and $r=\sqrt{4-M^2}$, i.e., at $(\tau_g,\delta_g)=(0,\pm\sqrt{4-M^2}/2)$; (iii) when $\beta_1>0$ and $\beta_2>0$, from the second equality, $f(\tau,\delta)$ attains its minimum when $r=0$, i.e., at $(\tau_g,\delta_g)=(0,0)$. From (2.31), the total energy $E(\tau,\delta)$ attains the minimum at the same (τ_g,δ_g). Then, from the proof of Lemma 2.1, one can obtain all real ground states $\boldsymbol{\xi}_g\in\mathbb{R}^5$ of (2.9) by direct calculations based on the four different parameter cases as shown in the proof of Lemma 2.1. In addition, from (2.7), τ and δ are, respectively, the values of F_+ and A_{00}, and hence according to the standard of classification in section 2.1, the phases of the ground states with parameters β_1,β_2 classified in (i), (ii), and (iii) are, respectively, ferromagnetic, nemati, and cyclic.

Above all, the real ground state $\boldsymbol{\xi}_g\in\mathbb{R}^5$ in a spatially uniform system can be thoroughly solved out and its phase category can also be identified. We summarize the results in Lemmas 2.3–2.5; the proofs follow directly the arguments stated above.

LEMMA 2.3. *When $\beta_1<0$ and $\beta_2>20\beta_1$, the ground state $\boldsymbol{\xi}_g$ is in the ferromagnetic phase, and for $M\in[0,2)$, it can be solved out as*

$$\boldsymbol{\xi}_g=\left(m_1^4/16,\ m_1^3m_2/8,\ \sqrt{6}m_1^2m_2^2/16,\ m_1m_2^3/8,\ m_2^4/16\right)^T, \tag{2.35}$$

with $m_1=\sqrt{2+M}$, $m_2=\sqrt{2-M}$.

LEMMA 2.4. *When $\beta_2<0$ and $\beta_2<20\beta_1$, the ground state $\boldsymbol{\xi}_g$ is in nematic phase. Moreover, if $0<M<2$, then $\boldsymbol{\xi}_g$ can be solved out as*

$$\boldsymbol{\xi}_g=(m_1/2,\ 0,\ 0,\ 0,\ m_2/2)^T; \tag{2.36}$$

and if $M=0$, $\boldsymbol{\xi}_g$ can be taken in two different types as

$$\begin{aligned}&\boldsymbol{\xi}_g=(\gamma_1\cos\theta,\ \gamma_1\sin\theta,\ \gamma,\ -\gamma_1\sin\theta,\ \gamma_1\cos\theta)^T \quad \text{or}\\ &\boldsymbol{\xi}_g=\left(\cos\theta/\sqrt{2},\ \sin\theta/\sqrt{2},\ 0,\ \sin\theta/\sqrt{2},\ -\cos\theta/\sqrt{2}\right)^T,\end{aligned} \tag{2.37}$$

where $\gamma_1=\sqrt{\frac{1-\gamma}{2}}$ for any γ with $|\gamma|\le 1$ and $\theta\in[0,2\pi)$.

LEMMA 2.5. *When $\beta_1>0$ and $\beta_2>0$, the ground state $\boldsymbol{\xi}_g$ is in the cyclic phase. Moreover, if $M\in[0,1]$, then $\boldsymbol{\xi}_g$ can be taken in three different types as*

$$\begin{aligned}&\boldsymbol{\xi}_g=\left(m_1^2/4,\ 0,\ \sqrt{2}\,m_1m_2/4,\ 0,\ m_2^2/4\right)^T \quad \text{or}\\ &\boldsymbol{\xi}_g=\left(\sqrt{3}\,m_3m_4/4,\ m_3^2/2,\ -\sqrt{2}\,m_3m_4/4,\ m_4^2/2,\ \sqrt{3}\,m_3m_4/4\right)^T \quad \text{or}\end{aligned} \tag{2.38}$$

$$\boldsymbol{\xi}_g=(\xi_2^g,\xi_1^g,\xi_0^g,\xi_{-1}^g,\xi_{-2}^g)^T, \tag{2.39}$$

where $m_3=\sqrt{1+M}$, $m_4=\sqrt{1-M}$, and

$$\begin{cases}\xi_0^g=-\frac{3\sqrt{6}}{8}M\sin^2\theta\cos\theta\mp-\frac{\sqrt{2}}{8}\big(2\cot(2\theta)+\cot\theta\big)g(\theta),\\ \xi_1^g=\frac{3}{4}M\sin^3\theta+\frac{1}{4}m_2^2\sin\theta\pm\frac{\sqrt{3}}{4}g(\theta), \qquad \xi_{-1}^g=\sin\theta-\xi_1^g,\\ \xi_2^g=\frac{1}{8}\big(3M\sin^2\theta+2m_1^2\big)\cos\theta\mp\frac{\sqrt{3}}{8}g(\theta)\tan\theta, \qquad \xi_{-2}^g=\xi_2^g-\cos\theta,\end{cases} \tag{2.40}$$

with $g(\theta)=\sqrt{\left(m_1m_2-3M^2\sin^2\theta\right)\sin^2\theta\cos^2\theta}$ *for* $\theta\in(0,2\pi)$ *satisfying* $|\sin\theta|\neq 1$ *and* $m_1m_2-3M^2\sin^2\theta\geq 0$. *If* $M\in(1,2)$, $\boldsymbol{\xi}_g$ *can only be taken as* (2.39).

Remark 2.2. For a spin-2 BEC in the spatially uniform system, i.e., under the ansatz (2.5), the minimization problem (2.2) collapses to

$$\tilde{\boldsymbol{\xi}}_g := \arg\min_{|\boldsymbol{\xi}|=1}\mathcal{E}_U(\boldsymbol{\xi}) = \arg\min_{M\in[-2,2]}\mathcal{E}_U(\boldsymbol{\xi}_g^M), \quad \text{with} \quad \boldsymbol{\xi}_g^M := \arg\min_{\boldsymbol{\xi}\in\mathbb{S}_C}\mathcal{E}_U(\boldsymbol{\xi}). \tag{2.41}$$

Define

$$\beta(M) := \mathcal{E}_U(\boldsymbol{\xi}_g^M), \qquad M\in[-2,2]. \tag{2.42}$$

By the results in Lemmas 2.3–2.5, we have for $M\in[-2,2]$

$$\beta(M) := \mathcal{E}_U(\boldsymbol{\xi}_g^M) = \frac{1}{2}\begin{cases} \beta_0+4\beta_1, & \beta_1<0\ \&\ \beta_2>20\beta_1,\\ \beta_0+\frac{\beta_2}{5}+\frac{(20\beta_1-\beta_2)M^2}{20}, & \beta_2<0\ \&\ \beta_2<20\beta_1,\\ \beta_0+\beta_1M^2, & \beta_1>0\ \&\ \beta_2>0.\end{cases} \tag{2.43}$$

Therefore, the energy of the ground state $\tilde{\boldsymbol{\xi}}_g$ defined in the minimization problem (2.41) is given as

$$\mathcal{E}_U(\tilde{\boldsymbol{\xi}}_g) = \min_{M\in[-2,2]}\beta(M) = \frac{1}{2}\begin{cases} \beta_0+4\beta_1, & \beta_1<0\ \&\ \beta_2>20\beta_1,\\ \beta_0+\beta_2/5, & \beta_2<0\ \&\ \beta_2<20\beta_1,\\ \beta_0, & \beta_1>0\ \&\ \beta_2>0.\end{cases} \tag{2.44}$$

This immediately suggests that, for the ground state of a spin-2 BEC defined as the minimizer of the energy functional under the total mass conservation, the ground state energy in a spatially uniform system is achieved in the nematic and cyclic phases when $M=0$ and, respectively, in the ferromagnetic phase for any $M\in[-2,2]$. The ground state is not unique. In fact, in the ferromagnetic phase, the ground state $\tilde{\boldsymbol{\xi}}_g$ can be taken as (2.35) for any $M\in[0,2]$, and in the nematic and cyclic phases, $\tilde{\boldsymbol{\xi}}_g$ can be taken as (2.37) and (2.38)–(2.39) with $M=0$, respectively.

2.3. Single mode approximation of ground states. In the literature [7, 29], the single mode approximation (SMA) is an interesting and useful tool for obtaining approximate ground states of spinor BEC. It can reduce solving the ground state of a spin-2 BEC to solving the ground state of a single component BEC. In fact, in the SMA for a spin-2 BEC, one assumes an ansatz for $\Phi\in\mathbb{S}$ in (1.4) as

$$\Phi(\boldsymbol{x}) = \phi(\boldsymbol{x})(\xi_2,\,\xi_1,\,\xi_0,\,\xi_{-1},\,\xi_{-2})^T =: \phi(\boldsymbol{x})\,\boldsymbol{\xi} =: \Phi_{\rm sma}(\boldsymbol{x}), \tag{2.45}$$

where $\boldsymbol{\xi}=(\xi_2,\,\xi_1,\,\xi_0,\,\xi_{-1},\,\xi_{-2})^T\in\mathbb{S}_C$ and $\phi:=\phi(\boldsymbol{x})\in\widetilde{\mathbb{S}}_1 := \{\varphi|\int_{\mathbb{R}^d}|\varphi(\boldsymbol{x})|^2d\boldsymbol{x}=1\}$. Plugging (2.45) into (1.1), noticing (2.6), we obtain

$$\mathcal{E}(\Phi) = \mathcal{E}(\Phi_{\rm sma}) = \int_{\mathbb{R}^d}\left[\frac{1}{2}|\nabla\phi|^2+V|\phi|^2+\mathcal{E}_U(\boldsymbol{\xi})|\phi|^4\right]d\boldsymbol{x} =: \mathcal{E}_{\rm sma}(\phi,\boldsymbol{\xi}). \tag{2.46}$$

Then the SMA of the ground state is to find $\Phi_{\rm sma}^g=\phi_g\,\boldsymbol{\xi}_g$ with $\boldsymbol{\xi}_g\in\mathbb{S}_C$ and $\phi_g\in\widetilde{\mathbb{S}}_1$ such that

$$\Phi_{\rm sma}^g := \arg\min_{\Phi_{\rm sma}\in\mathbb{S}}\mathcal{E}(\Phi_{\rm sma}). \tag{2.47}$$

Combining (2.47), (2.46), (2.41), and (2.42), we get

$$\begin{aligned}\mathcal{E}(\Phi^g_{\rm sma}) &= \min_{\Phi_{\rm sma}\in\mathbb{S}} \mathcal{E}(\Phi_{\rm sma}) = \min_{\phi\in\widetilde{\mathbb{S}}_1}\min_{\boldsymbol{\xi}\in\mathbb{S}_C} \mathcal{E}_{\rm sma}(\phi,\boldsymbol{\xi})\\ &= \min_{\phi\in\widetilde{\mathbb{S}}_1}\left\{\int_{\mathbb{R}^d}\left[\frac{1}{2}|\nabla\phi|^2+V|\phi|^2+\left(\min_{\boldsymbol{\xi}\in\mathbb{S}_C}\mathcal{E}_U(\boldsymbol{\xi})\right)|\phi|^4\right]d\boldsymbol{x}\right\} = \min_{\phi\in\widetilde{\mathbb{S}}_1} E_{\rm sma}(\phi),\end{aligned}$$

where

$$E_{\rm sma}(\phi) = \int_{\mathbb{R}^d}\left[\frac{1}{2}|\nabla\phi|^2+V|\phi|^2+\beta(M)\,|\phi|^4\right]d\boldsymbol{x}. \tag{2.48}$$

Thus $\boldsymbol{\xi}_g$ is the ground state of a spin-2 BEC in a spatially uniform system, i.e., (2.9), and ϕ_g is the ground state of a singe-component BEC, i.e.,

$$\phi_g := \arg\min_{\phi\in\widetilde{\mathbb{S}}_1} E_{\rm sma}(\phi). \tag{2.49}$$

As it has been observed numerically and proved mathematically in the literature [7, 29], the above SMA of the ground state indeed gives the ground state of the spin-2 BEC in the following cases: (i) when $M = \pm 2$, (ii) when $M = 0$, and (iii) in ferromagnetic phase when $\beta_1 < 0$ and $\beta_2 > 20\beta_1$ for $M \in [-2, 2]$. Thus, in these cases, the computation of the ground state of a spin-2 BEC can be reduced to the computation of the ground state of a single component BEC, i.e., (2.49). Certainly, for all the other cases, one has to solve the original minimization problem (1.4).

3. An efficient and accurate numerical method. In this section, we first present a normalized gradient flow (NGF) to compute the ground state of the spin-2 BEC, we then introduce three additional equations for determining the five projection constants in the projection step for semidiscretization of the NGF in time, and finally a full discretization of the NGF is proposed.

3.1. A continuous normalized gradient flow (CNGF). In order to compute the ground state of spin-2 BEC (1.4), similarly to the single-component BEC [6, 11] and spin-1 BEC [6, 13], here we first present a continuous normalized gradient flow (CNGF) for $\Phi := \Phi(\boldsymbol{x},t) = (\phi_2,\phi_1,\phi_0,\phi_{-1},\phi_{-2})^T := (\phi_2(\boldsymbol{x},t),\phi_1(\boldsymbol{x},t),\phi_0(\boldsymbol{x},t),$ $\phi_{-1}(\boldsymbol{x},t),\phi_{-2}(\boldsymbol{x},t))^T$ as [38]

$$\partial_t\phi_\ell = -[H_\rho + a_\ell(\Phi)]\phi_\ell - f_\ell(\Phi) + [\mu_\Phi(t)+\ell\lambda_\Phi(t)]\phi_\ell =: \big(\mathbf{H}\Phi\big)_\ell,\ \ -2\le\ell\le 2, \tag{3.1}$$

where $a_\ell := a_\ell(\Phi)$ and $f_\ell := f_\ell(\Phi)$ ($\ell = 2,\ldots,-2$) are given as

$$\begin{aligned} a_0 &= 3\beta_1(|\phi_1|^2+|\phi_{-1}|^2)+0.2\beta_2|\phi_0|^2,\\ f_0 &= \beta_1\left[\left(\frac{\sqrt{6}}{2}F_+ - 3\bar{\phi}_1\phi_0\right)\phi_1 + \left(\frac{\sqrt{6}}{2}F_- - 3\bar{\phi}_{-1}\phi_0\right)\phi_{-1}\right] + \beta_2\left(\frac{A_{00}}{\sqrt{5}}+0.2\beta_2\phi_0^2\right)\bar{\phi}_0,\\ a_{\pm\ell} &= \beta_1\left[2\,|\phi_{\pm(3-\ell)}|^2 \pm \ell\,F_z(\Phi) + (6-3\ell)\,|\phi_0|^2\right] + 0.4\beta_2|\phi_{\mp\ell}|^2, \qquad \ell = 2,1,\\ f_{\pm\ell} &= \beta_1\Big\{\left[(\ell-1)F_\mp + (2-\ell)F_\pm - 2\,\bar{\phi}_{\pm(3-\ell)}\phi_{\pm\ell}\right]\phi_{\pm(3-\ell)}\\ &\quad + (2-\ell)\left[\frac{\sqrt{6}}{2}F_\mp - 3\bar{\phi}_0\phi_{\pm\ell}\right]\phi_0\Big\} + \beta_2\left[\frac{(-1)^\ell A_{00}}{\sqrt{5}} - 0.4\phi_{\pm\ell}\phi_{\mp\ell}\right]\bar{\phi}_{\mp\ell}, \quad \ell = 2,1.\end{aligned}$$

Here, $\mu_\Phi(t)$ and $\lambda_\Phi(t)$ are the Lagrangian multipliers such that both the mass (1.2) and the magnetization (1.3) are conserved during dynamics and they can be taken as [38]

$$\begin{cases} \mu_\Phi(t) = \dfrac{\mathcal{R}(\Phi(\boldsymbol{x},t))\,\mathcal{K}(\Phi(\boldsymbol{x},t)) - \mathcal{M}(\Phi(\boldsymbol{x},t))\,\mathcal{P}(\Phi(\boldsymbol{x},t))}{\mathcal{R}(\Phi(\boldsymbol{x},t))\,\mathcal{N}(\Phi(\boldsymbol{x},t)) - \mathcal{M}^2(\Phi(\boldsymbol{x},t))}, \\ \lambda_\Phi(t) = \dfrac{\mathcal{N}(\Phi(\boldsymbol{x},t))\,\mathcal{P}(\Phi(\boldsymbol{x},t)) - \mathcal{M}(\Phi(\boldsymbol{x},t))\,\mathcal{K}(\Phi(\boldsymbol{x},t))}{\mathcal{R}(\Phi(\boldsymbol{x},t))\,\mathcal{N}(\Phi(\boldsymbol{x},t)) - \mathcal{M}^2(\Phi(\boldsymbol{x},t))}, \end{cases} \tag{3.2}$$

with $\mathcal{N}(\Phi(\boldsymbol{x},t))$ and $\mathcal{M}(\Phi(\boldsymbol{x},t))$ given in (1.2) and (1.3), respectively, and

$$\mathcal{R}(\Phi(\boldsymbol{x},t)) = \sum_{\ell=-2}^{2} \ell^2 \|\phi_\ell(\boldsymbol{x},t)\|^2, \quad \mathcal{K}(\Phi(\boldsymbol{x},t)) = \sum_{\ell=-2}^{2} \int_{\mathbb{R}^d} \bar{\phi}_\ell(\boldsymbol{x},t) \left(\mathbf{H}\Phi\right)_{-\ell}(\boldsymbol{x},t)\, d\boldsymbol{x},$$
$$\mathcal{P}(\Phi(\boldsymbol{x},t)) = \sum_{\ell=-2}^{2} \int_{\mathbb{R}^d} \ell\, \bar{\phi}_\ell(\boldsymbol{x},t) \left(\mathbf{H}\Phi\right)_{-\ell}(\boldsymbol{x},t)\, d\boldsymbol{x}, \qquad t \geq 0.$$

For any given initial data $\Phi(\boldsymbol{x},0) := \Phi_0(\boldsymbol{x})$ satisfying

$$\mathcal{N}(\Phi_0(\boldsymbol{x})) = 1, \qquad \mathcal{M}(\Phi_0(\boldsymbol{x})) = M, \tag{3.3}$$

it is easy to show that the CNGF (3.1) conserves the total mass and magnetization while diminishing the total energy [38], i.e.,

$$\begin{aligned} &\mathcal{N}(\Phi(\cdot,t)) \equiv \mathcal{N}(\Phi_0) = 1, \qquad \mathcal{M}(\Phi(\cdot,t)) \equiv \mathcal{M}(\Phi_0) = M, \qquad t \geq 0, \\ &\mathcal{E}(\Phi(\cdot,t)) \leq \mathcal{E}(\Phi(\cdot,s)) \leq \mathcal{E}(\Phi_0) \qquad \forall\, t \geq s \geq 0. \end{aligned} \tag{3.4}$$

Thus the ground state of spin-2 BEC (1.4) can be obtained as the steady state of the CNGF (3.1) with proper choice of the initial data Φ_0 satisfying (3.3).

3.2. A gradient flow with discrete normalization (GFDN). Choose a time step size $\Delta t > 0$, and denote time steps as $t_n = n\Delta t$ for $n \geq 0$. Then a gradient flow with discrete normalization (GFDN) for computing the ground state of the spin-2 BEC (1.4) can be constructed by first applying the first-order time-splitting semidiscretization of the CNGF (3.1) as

$$\partial_t \phi_\ell = -\left(H_\rho + a_\ell(\Phi)\right)\phi_\ell - f_\ell(\Phi), \quad t \in [t_{n-1}, t_n), \quad \ell = 2, 1, \ldots, -2, \tag{3.5}$$

followed by a projection step as

$$\phi_\ell(\boldsymbol{x}, t_n) := \phi_\ell(\boldsymbol{x}, t_n^+) = \sigma_\ell^n \phi_\ell(\boldsymbol{x}, t_n^-), \qquad \ell = 2, 1, \ldots, -2. \tag{3.6}$$

Here, $\phi_\ell(\boldsymbol{x}, t_n^\pm) = \lim_{t \to t_n^\pm} \phi_\ell(\boldsymbol{x}, t)$. Moreover, the projection constants $\sigma_\ell^n \geq 0$ for $\ell = 2, 1, \ldots, -2$ are to be chosen such that

$$\|\Phi(\cdot, t_n)\|^2 = \sum_{\ell=-2}^{2} \|\phi_\ell(\cdot, t_n)\|^2 = 1, \qquad \sum_{\ell=-2}^{2} \ell \|\phi_\ell(\cdot, t_n)\|^2 = M. \tag{3.7}$$

Plugging (3.6) into (3.7), we have

$$\sum_{\ell=-2}^{2} (\sigma_\ell^n)^2 \|\phi_\ell(\cdot, t_n^-)\|^2 = 1, \qquad \sum_{\ell=-2}^{2} \ell (\sigma_\ell^n)^2 \|\phi_\ell(\cdot, t_n^-)\|^2 = M. \tag{3.8}$$

In fact, in the projection step, we have to determine the five projection constants σ_ℓ^n for $\ell = 2, \ldots, -2$ in (3.6). However, we only have two equations in (3.8). In order to find additional proper constraints for determining the five projection constants in projection step (3.6), we can view the GFDN (3.5)–(3.6) as a first-order time-splitting semidiscretization of the CNGF (3.1). In this regard, the projection step (3.6) is similar to solving the following nonlinear ordinary differential equations (ODEs):

$$\partial_t \phi_\ell(\boldsymbol{x}, t) = [\mu_\Phi(t) + \ell\lambda_\Phi(t)]\phi_\ell, \quad t_{n-1} \le t \le t_n, \quad \ell = 2, 1, \ldots, -2. \tag{3.9}$$

Solving the above ODEs, one obtains for $\ell = 2, 1, \ldots, -2$ that

$$\phi_\ell(\boldsymbol{x}, t_n) = \phi_\ell(\boldsymbol{x}, t_{n-1}) \exp\left(\int_{t_{n-1}}^{t_n} [\mu_\Phi(s) + \ell\lambda_\Phi(s)]\ ds\right) := \tilde{\sigma}_\ell^n \phi_\ell(\boldsymbol{x}, t_{n-1}), \tag{3.10}$$

which suggests the following three relationships for the constants $\tilde{\sigma}_\ell^n$ ($\ell = 2, 1, \ldots, -2$):

$$\tilde{\sigma}_2^n \tilde{\sigma}_{-2}^n = (\tilde{\sigma}_0^n)^2, \qquad \tilde{\sigma}_1^n \tilde{\sigma}_{-1}^n = (\tilde{\sigma}_0^n)^2, \qquad \tilde{\sigma}_2^n \tilde{\sigma}_0^n = (\tilde{\sigma}_1^n)^2. \tag{3.11}$$

Based on the above observation, we propose and adapt the following three additional constraints for determining the five projection constants in the project step (3.6) as

$$\sigma_2^n \sigma_{-2}^n = (\sigma_0^n)^2, \qquad \sigma_1^n \sigma_{-1}^n = (\sigma_0^n)^2, \qquad \sigma_2^n \sigma_0^n = (\sigma_1^n)^2. \tag{3.12}$$

For the existence and uniqueness (in most cases) of the five project constants $\sigma_\ell^n \ge 0$ for $\ell = 2, 1, \ldots, -2$ governed by (3.8) and (3.12), we have the following result.

THEOREM 3.1. *For sufficiently small time step size $\Delta t > 0$ and for all $M \in [0, 2)$, the solution σ_ℓ^n ($\ell = 2, \ldots, -2$) satisfying (3.8) and (3.12) can be solved out as follows:*

(i) *when $M = 1$, $\|\phi_1(\boldsymbol{x}, t_n^-)\| > 0$, and $\|\phi_\ell(\boldsymbol{x}, t_n^-)\| = 0$ ($\ell = 2, 0, -1, -2$), then*

$$\sigma_1^n = \frac{1}{\|\phi_1(\boldsymbol{x}, t_n^-)\|}, \qquad \sigma_0^n = 1, \qquad \sigma_\ell^n = (\sigma_1^n)^\ell, \quad \ell = 2, -1, -2; \tag{3.13}$$

(ii) *when $M = 0$, $\|\phi_0(\boldsymbol{x}, t_n^-)\| > 0$, and $\|\phi_\ell(\boldsymbol{x}, t_n^-)\| = 0$ ($\ell = 2, 1, -1, -2$), then*

$$\sigma_0^n = \frac{1}{\|\phi_0(\boldsymbol{x}, t_n^-)\|}, \qquad \sigma_1^n = 1, \qquad \sigma_\ell^n = (\sigma_0^n)^{1-\ell}, \quad \ell = 2, -1, -2; \tag{3.14}$$

(iii) *for all other cases, then*

$$\sigma_0^n = \frac{1}{\sqrt{\sum_{\ell=-2}^{2} \lambda_*^\ell \|\phi_\ell(\boldsymbol{x}, t_n^-)\|^2}}, \qquad \sigma_\ell^n = \sigma_0^n (\lambda_*)^{\ell/2}, \tag{3.15}$$

for $\ell = -2, -1, 1, 2,$. Here, λ_* is the unique positive solution of the following fourth-order algebraic equation with respect to the unknown λ as

$$\sum_{\ell=-2}^{2} (\ell - M)\|\phi_\ell(\boldsymbol{x}, t_n^-)\|^2 \lambda^{\ell+2} = 0. \tag{3.16}$$

Proof. Combining (3.8) and (3.12), it is straightforward to check that (3.13) is a solution (not unique) of (3.8) and (3.12) in case (i), and (3.14) is a solution (not unique) of (3.8) and (3.12) in case (ii).

Now we prove (3.15) in case (iii). Noticing (3.7) is also valid when t_n is replaced by t_{n-1} for $n \geq 1$, i.e.,

$$\sum_{\ell=-2}^{2} \|\phi_\ell(\boldsymbol{x}, t_{n-1})\|^2 = 1, \qquad \sum_{\ell=-2}^{2} \ell \|\phi_\ell(\boldsymbol{x}, t_{n-1})\|^2 = M, \tag{3.17}$$

we have

$$\sum_{\ell=-2}^{2} (\ell - M) \|\phi_\ell(\boldsymbol{x}, t_{n-1})\|^2 = 0. \tag{3.18}$$

In addition, for sufficiently small time step size $\Delta t > 0$, $\|\phi_\ell(\cdot, t)\| \in \mathcal{C}([t_{n-1}, t_n))$ $(\ell = 2 \ldots, -2)$ implies

$$\|\phi_\ell(\boldsymbol{x}, t_{n-1})\| > 0 \qquad \Longleftrightarrow \qquad \|\phi_\ell(\boldsymbol{x}, t_n^-)\| > 0. \tag{3.19}$$

Combining (3.19) and (3.17), we get $\sum_{\ell=-2}^{2} \|\phi_\ell(\boldsymbol{x}, t_n^-)\|^2 > 0$. Therefore, case (iii) can be divided into three subcases:

(a) $M = 1$ and $\|\phi_2(\boldsymbol{x}, t_n^-)\| + \|\phi_0(\boldsymbol{x}, t_n^-)\| + \|\phi_{-1}(\boldsymbol{x}, t_n^-)\| + \|\phi_{-2}(\boldsymbol{x}, t_n^-)\| > 0$.

(b) $M = 0$ and $\|\phi_2(\boldsymbol{x}, t_n^-)\| + \|\phi_1(\boldsymbol{x}, t_n^-)\| + \|\phi_{-1}(\boldsymbol{x}, t_n^-)\| + \|\phi_{-2}(\boldsymbol{x}, t_n^-)\| > 0$.

(c) $M \neq 1$ and $M \neq 0$; thus $\ell - M \neq 0$ $(\ell = 2, \ldots, -2)$ by noticing $M \in [0, 2)$.

For all three subcases (a)–(c), noting (3.18)–(3.19), it holds that

$$\sum_{\ell < M} \|\phi_\ell(\boldsymbol{x}, t_n^-)\|^2 > 0, \qquad \sum_{\ell > M} \|\phi_\ell(\boldsymbol{x}, t_n^-)\|^2 > 0. \tag{3.20}$$

Denote $\lambda = \sigma_2^n / \sigma_0^n$, by (3.8) and (3.12); for any $M \in [0, 2)$, we have

$$\begin{cases} \sigma_0^n = \dfrac{1}{\sqrt{\sum_{\ell=-2}^{2} \|\phi_\ell(\boldsymbol{x}, t_n^-)\|^2 \lambda^\ell}}, \qquad \sigma_j^n = \sigma_0^n \lambda^{j/2}, \quad j = 2, 1, -1, -2, \\ g(\lambda) := \displaystyle\sum_{\ell=-2}^{2} (\ell - M) \|\phi_\ell(\boldsymbol{x}, t_n^-)\|^2 \lambda^{\ell+2} = 0. \end{cases} \tag{3.21}$$

Then we need only to show that $g(\lambda)$ has a unique positive root to finish the proof.

Define ℓ_1^n, $\ell_2^n \in \{2, 1, 0, -1, -2\}$ as

$$\ell_1^n := \min\{\ell \mid \|\phi_\ell(\boldsymbol{x}, t_n^-)\| \neq 0\} < \ell_2^n := \max\{\ell \mid \|\phi_\ell(\boldsymbol{x}, t_n^-)\| \neq 0\}.$$

Then (3.20) indicates that $\ell_1^n < M$ and $\ell_2^n > M$. Hence, $g(\lambda)$ can be reformulated as

$$\begin{aligned} g(\lambda) &= \sum_{\ell_1^n \leq \ell < M} (\ell - M) \|\phi_\ell(\boldsymbol{x}, t_n^-)\|^2 \lambda^{\ell+2} + \sum_{M < \ell \leq \ell_2^n} (\ell - M) \|\phi_\ell(\boldsymbol{x}, t_n^-)\|^2 \lambda^{\ell+2} \\ &=: h(\lambda) \lambda^{\ell_1^n + 2}, \end{aligned}$$

where

$$\begin{aligned} h(\lambda) &= \sum_{\ell_1^n \leq \ell < M} (\ell - M) \|\phi_\ell(\boldsymbol{x}, t_n^-)\|^2 \lambda^{\ell - \ell_1^n} + \sum_{M < \ell \leq \ell_2^n} (\ell - M) \|\phi_\ell(\boldsymbol{x}, t_n^-)\|^2 \lambda^{\ell - \ell_1^n} \\ &=: h_1(\lambda) + h_2(\lambda). \end{aligned}$$

A simple calculation shows that

$$\lim_{\lambda\to 0^+} h(\lambda) = (\ell_1^n - M)\|\phi_{\ell_1^n}(\boldsymbol{x},t_n^-)\|^2 < 0, \qquad\qquad \lim_{\lambda\to +\infty} h(\lambda) = +\infty,$$

which immediately implies that $h(\lambda)$ has at least one positive root $\lambda_* > 0$. In addition, at any positive root $\lambda = \lambda_* > 0$ of $h(\lambda)$, noticing (3.20), we have

$$\begin{aligned}
h'(\lambda_*) =& h_1'(\lambda_*) + h_2'(\lambda_*)\\
=& \sum_{\ell_1^n \le \ell < M} (\ell - \ell_1^n)\,(\ell - M)\|\phi_\ell(\boldsymbol{x},t_n^-)\|^2(\lambda_*)^{\ell-\ell_1^n-1} + h_2'(\lambda_*)\\
=& \lambda_*^{-1}\,(M-\ell_1^n) \sum_{\ell_1^n \le \ell < M} (\ell - M)\|\phi_\ell(\boldsymbol{x},t_n^-)\|^2(\lambda_*)^{\ell-\ell_1^n} + h_2'(\lambda_*)\\
=& \lambda_*^{-1}\,(M-\ell_1^n)\, h_1(\lambda_*) + h_2'(\lambda_*)\\
=& \lambda_*^{-1}\,(M-\ell_1^n)\left[h(\lambda_n) - h_2(\lambda_*)\right] + h_2'(\lambda_*) = \lambda_*^{-1}\,(\ell_1^n - M)\, h_2(\lambda_*) + h_2'(\lambda_*)\\
=& \sum_{M<\ell\le \ell_2^n} (\ell_1^n - M)\,(\ell - M)\|\phi_\ell(\boldsymbol{x},t_n^-)\|^2(\lambda_*)^{\ell-\ell_1^n-1} + h_2'(\lambda_*)\\
=& \sum_{M<\ell\le \ell_2^n} \left[(\ell-M)^2 - (\ell-\ell_1^n)\,(\ell-M)\right]\|\phi_\ell(\boldsymbol{x},t_n^-)\|^2(\lambda_*)^{\ell-\ell_1^n-1} + h_2'(\lambda_*)\\
=& \sum_{M<\ell\le \ell_2^n} (\ell-M)^2\|\phi_\ell(\boldsymbol{x},t_n^-)\|^2(\lambda_*)^{\ell-\ell_1^n-1} > 0.
\end{aligned}$$

Therefore, $h(\lambda)$ (and thus $g(\lambda)$) has exactly one positive root λ_*. Substituting $\lambda = \lambda_*$ into (3.21) leads to the formulas for the projection constants in (3.15). ∎

3.3. A backward-forward Euler finite difference discretization. Due to the trapping potential $V(\boldsymbol{x})$, the solution $\Phi(\boldsymbol{x},t)$ of the CNGF (3.1) (or the GFDN (3.5)–(3.6)) decays exponentially fast to zero as $|\boldsymbol{x}| \to \infty$. Hence, one can truncate the problem into a bounded domain $\mathcal{D}$ with the homogeneous Dirichlet boundary condition in practical computation. Various methods, such as the backward (-forward) Euler finite difference/sine-spectral method [9, 11, 13], can be applied to discretize the GFDN (3.5)–(3.6). In this section, we adapt a backward-forward Euler finite difference method (BEFD) to discretize the GFDN (3.5)–(3.6).

To simplify the presentation, we introduce the scheme for the case of one spatial dimension, i.e., $d=1$, defined on an interval $\mathcal{D} = (a,b)$ with the homogeneous Dirichlet boundary condition. Generalization to higher dimension is straightforward by tensor product. For $d=1$, the spatial mesh size is chosen as $h = (b-a)/N$, with N an even positive integer. Let $x_j := a + jh,\ j = 0,\ldots,N$ be the grid points, and denote, respectively, Φ_j^n and ρ_j^n as the approximation of $\Phi(x_j,t_n)$ and $\rho(x_j,t_n)$. Moreover, we denote Φ^n as the solution vector with component Φ_j^n. Then the GFDN (3.5)–(3.6) is discretized as

$$\begin{cases} \dfrac{\phi_{\ell,j}^* - \phi_{\ell,j}^n}{\Delta t} = \left(\dfrac{1}{2}\delta_h^2 - V_j - \rho_j^n - a_\ell(\Phi_j^n)\right)\phi_{\ell,j}^* - f_\ell(\Phi_j^n), & 1 \le j \le N-1,\\ \phi_{\ell,j}^{n+1} = \sigma_\ell^n\,\phi_{\ell,j}^*, \qquad \ell = 2,\ldots,-2, & j = 0,1,\ldots,N. \end{cases} \tag{3.22}$$

Here, $V_j = V(x_j)$, δ_h^2 is the second-order central finite difference operator, and $\sigma_\ell^n(\ell = 2,\ldots,-2)$ are the projection constants chosen as (3.13)–(3.15). In addition, the homogeneous Dirichlet boundary condition and initial data are discretized as

$$\phi_{\ell,0}^* = \phi_{\ell,N}^* = 0, \qquad \phi_{\ell,j}^0 = \phi_\ell(x_j,0), \qquad \ell = 2,\ldots,-2, \quad j = 0,1,\ldots,N. \tag{3.23}$$

4. Numerical results. In this section, we first study how to choose proper initial data for computing numerically the ground states of spin-2 BECs and then apply the numerical method to compute the ground states under different interaction parameters β_1 and β_2 as well as the magnetization M in one and two dimensions. Uniqueness and nonuniqueness of the ground state are tested and discussed based on our extensive numerical results. In our numerical computations, the ground state $\Phi_g := \lim_{n\to\infty} \Phi^n$ is reached numerically when $\frac{\|\Phi^{n+1}-\Phi^n\|_\infty}{\Delta t} \le \varepsilon := 10^{-7}$.

In practice, unless stated, we fix $\beta_0 = 100$, $\Delta t = 0.005$, and $\mathcal{D} = [-10, 10]^d$ for $d = 1, 2$. The mesh size is taken as $h_x = 1/64$ when $d = 1$ and, respectively, $h_x = h_y = 1/16$ when $d = 2$. Moreover, $V(\boldsymbol{x})$ is chosen either as the harmonic plus optical lattice potential

$$V(\boldsymbol{x}) = \sum_{j=1}^{d} \left[\frac{1}{2}\nu_j^2 + \eta\,(d-1)\sin^2(q_j\nu_j)\right], \quad \boldsymbol{x} \in \mathcal{D}, \quad d = 1, 2, \tag{4.1}$$

with $\nu_1 = x$, $\nu_2 = y$, η, and q_j $(j = 1, 2)$ given constants, or the box potential

$$V_{\mathrm{box}}(\boldsymbol{x}) = \begin{cases} 0, & \boldsymbol{x} \in \mathcal{D}, \\ +\infty & \text{otherwise}. \end{cases} \tag{4.2}$$

4.1. Choice of initial data and uniqueness of the ground state. A proper choice of initial data $\Phi_0(\boldsymbol{x})$ usually improves significantly the efficiency and accuracy of the GFDN (3.5)–(3.6). For cases where SMA is valid, e.g., the nematic phase with $M = 0$ and the ferromagnetic phase [7] (see also Figure 4.4), one can either simply construct the ground state via (2.49) by solving the ground state of the single component BEC (2.49) or directly solve the ground state via the GFDN (3.22)–(3.6) with initial data (it is a reasonable and natural choice by noticing section 2.3) taken as

$$\boldsymbol{\Phi}_0(\boldsymbol{x}) = \boldsymbol{\xi}_g\, \phi(\boldsymbol{x}), \tag{4.3}$$

where $\boldsymbol{\xi}_g$ is given in Lemmas 2.3–2.5 and $\phi(\boldsymbol{x})$ is an approximation of the ground state of the single component BEC (2.49), e.g., the harmonic oscillator approximation $\phi_g^{\mathrm{hos}}(\boldsymbol{x})$ for small $\beta(M)$ and/or the Thomas–Fermi approximation $\phi_g^{\mathrm{TF}}(\boldsymbol{x})$ for large $\beta(M)$ [11, 13]. For other cases where the SMA is invalid, the initial data Φ_0 can be chosen either as (4.3) or as a more general initial setup:

$$\boldsymbol{\Phi}^0(\boldsymbol{x}) = \phi(\boldsymbol{x})\boldsymbol{\xi} =: \frac{\phi(\boldsymbol{x})}{2}\left(\sqrt{2+M-2\sigma},\, \sqrt{\sigma},\, \sqrt{2\sigma},\, \sqrt{\sigma},\, \sqrt{2-M-2\sigma}\right)^T, \tag{4.4}$$

with $\sigma \in [0, 1 - M/2]$. Extensive numerical comparison (not shown here for brevity) for different initial data shows that the GFDN would usually converge faster with initial data (4.3) than with other types of initial data. Based on those comparisons, we would conclude and suggest the choice of initial data as follows:

(a) For the ferromagnetic phase, $\boldsymbol{\xi}_g$ is suggested to be chosen as (2.35) for all $M \in [0, 2)$. Meanwhile, the ground state is found to be unique.

(b) For the nematic phase, if $M \in (0, 2)$, $\boldsymbol{\xi}_g$ is suggested to be chosen as (2.36); the ground state is found to be unique. However, if $M = 0$, the ground state is not unique. Hence, any initial data chosen as (2.36) works and probably converges to different ground states.

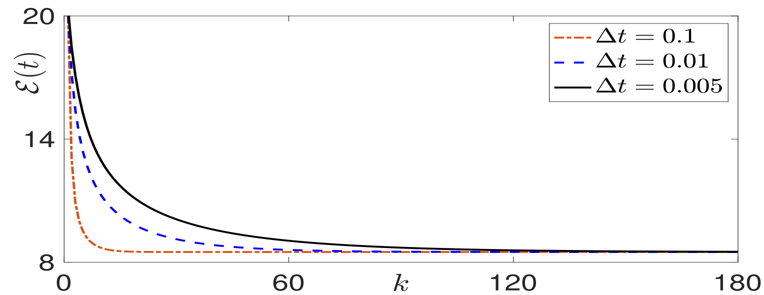

FIG. 4.1. *Time evolution of the total energy $\mathcal{E}(t)$ in Example* 4.1 *with different time step size Δt.*

(c) For the cyclic phase, if $M \in (0,2)$, then $\boldsymbol{\xi}_g$ is suggested to be chosen as (2.39) with $\theta = \arctan\sqrt{(2-M)/(1+M)}$, i.e.,

$$\boldsymbol{\xi}_g = \left(\sqrt{(M+1)/3},\ 0,\ 0,\ \sqrt{(2-M)/3},\ 0\right)^T. \tag{4.5}$$

The ground state is found to be unique, which is essentially different from the spatially uniform system where the ground state is not unique. While if $M = 0$, similar to the nematic phase, the ground state is not unique, and thus any initial data works and probably converges to different ground states.

Example 4.1. Here we show the energy-diminishing property of our numerical method. To this end, we let $M = 0.5$, $\beta_1 = 1$, and $\beta_2 = -2$ (i.e., the nematic phase). The ground state of a spin-2 BEC is computed by the BEFD (3.22) with time step $\Delta t = 0.1/0.01/0.005$ and the initial data (4.4) with $\sigma = 0$; i.e., $\boldsymbol{\xi}$ is chosen as the ground state in a spatially uniform system (2.36). Figure 4.1 shows the evolution of the energy $\mathcal{E}(t) := \mathcal{E}(\Phi(\cdot, t))$ with different time step Δt.

From Figure 4.1 and additional experiments not shown here for brevity, we can see that (i) the energy is diminishing for different time step size Δt, even for the relatively large step size $\Delta t = 0.1$ (cf. Figure 4.1), and (ii) the GFDN with different initial data converges to the same ground state. In addition, when $\sigma = 0$, i.e., $\boldsymbol{\xi}$ is chosen as the ground state in a spatially uniform system (2.36), the GFDN usually converges in the fastest way.

4.2. Applications. In this subsection, we apply our numerical method to compute the ground state of a spin-2 BEC with different parameter regimes.

Example 4.2. Here we further study the nonuniqueness of the ground state under some parameter regimes. We take $d = 1$ and carry out the following cases:

(i) Case 1. $\beta_1 = -1$, $\beta_2 = -20$, $M = 0.5$, and $\boldsymbol{\xi}_g$ is taken as (2.35) and (2.36), respectively.

(ii) Case 2. $\beta_1 = 0$, $\beta_2 = 1$, $M = 0.8$, and $\boldsymbol{\xi}_g$ is taken as (2.35) and (4.5), respectively.

(iii) Case 3. $\beta_1 = 10$, $\beta_2 = 2$, $M = 0$, and $\boldsymbol{\xi}_g$ is taken as (2.38) and (2.39) with $\theta = \arcsin(1/5)$, respectively.

(iv) Case 4. $\beta_1 = 1$, $\beta_2 = -2$, $M = 0$, and $\boldsymbol{\xi}_g$ is taken as (2.37) with ($\gamma_1 = 0.4, \theta = \arcsin\sqrt{2/15}$) and $\theta = \arcsin(2\sqrt{2}/5)$, respectively.

Figure 4.2 depicts the wave functions of different ground states computed by different initial data in Cases 1–4. For each case, different initial data converges to

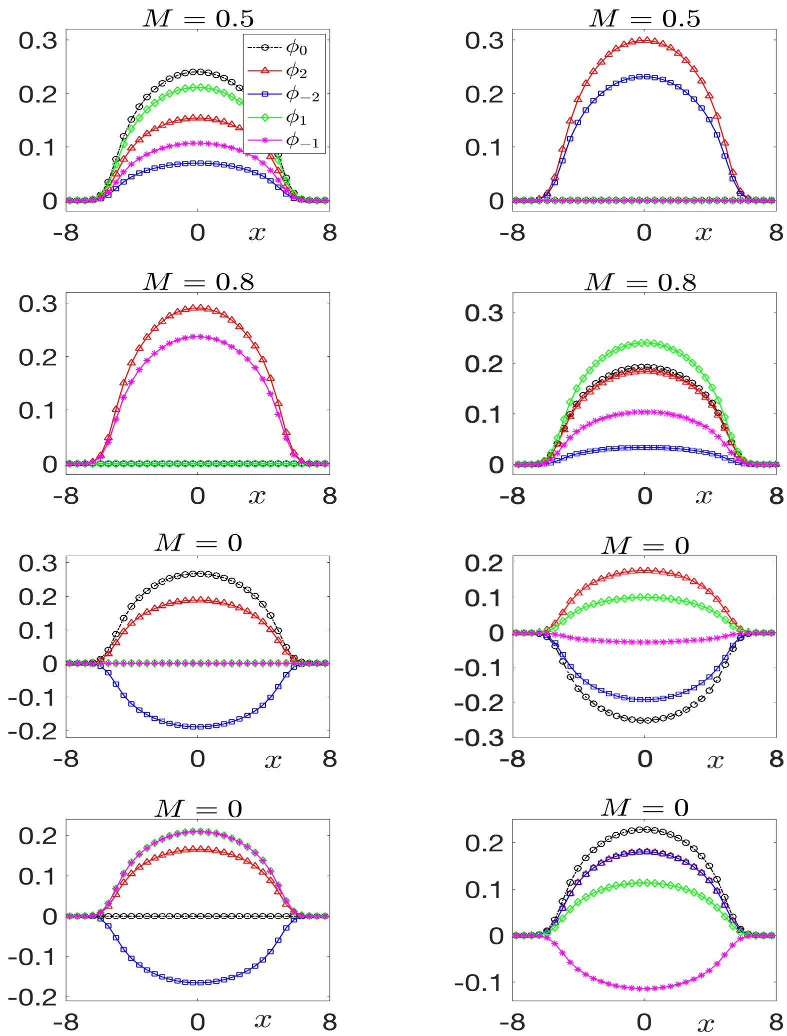

FIG. 4.2. *Plots of the wave function of the ground states ϕ_ℓ $(\ell = 2, 1, 0, -1, -2)$ in Cases* 1–4 *(from top to bottom) that were computed by different initial data in Example* 4.2.

different ground states with the same energy, which are $\mathcal{E}(\Phi^g) = 8.28198899$, 8.50852656, 8.50852656, and 8.48600868 for Cases 1–4, respectively. From Figure 4.2 and additional results not shown here for brevity, we can see that the ground states are not unique for the following four cases (cf. Figure 4.2): (a) for all $M \in [0, 2)$ and $\beta_1 < 0$, $\beta_2 = 20\beta_1$. (b) for all $M \in [0, 2)$ and $\beta_2 > 0$, $\beta_1 = 0$. (c) $M = 0$ and $\beta_1 > 0$, $\beta_2 > 0$. (d) $M = 0$ and $\beta_2 < 0$, $\beta_2 < 20\beta_1$.

Example 4.3. In order to study the wave functions and the SMA property of the ground states in different parameter regimes, we take $d = 1$, the initial data as (4.3) with $\boldsymbol{\xi}_g$ reading as (2.35), (2.36), and (4.5), and consider following three cases:

(i) Case 5. ferromagnetic phase: we take $\beta_1 = -1$ and $\beta_2 = 2$.
(ii) Case 6. nematic phase: we choose $\beta_1 = 1$ and $\beta_2 = -2$.
(iii) Case 7. cyclic phase: we let $\beta_1 = 10$ and $\beta_2 = 2$.

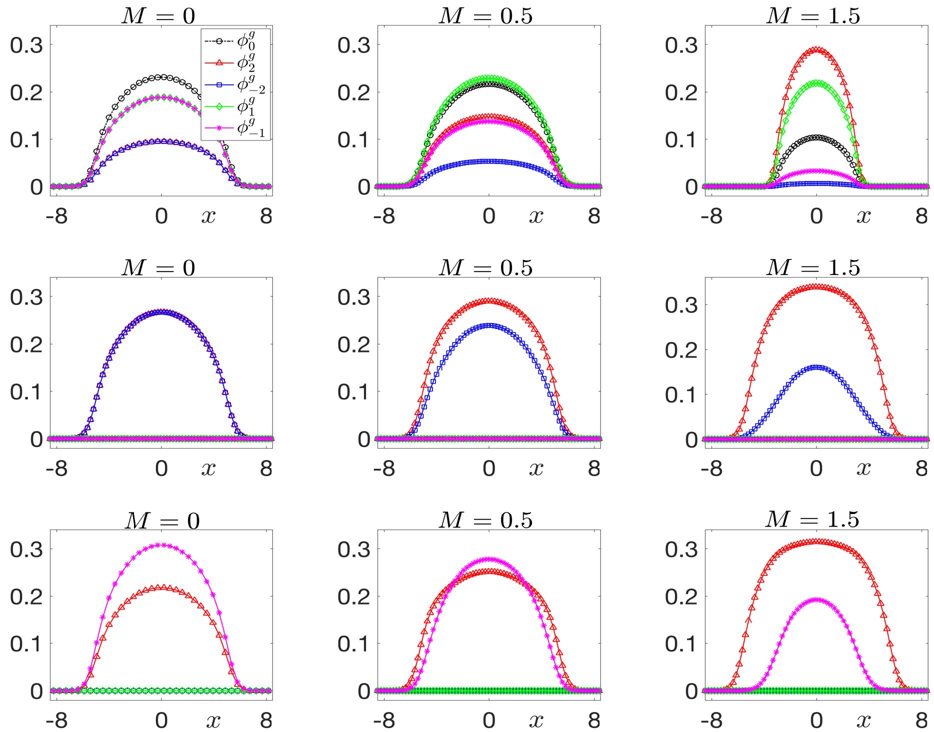

Fig. 4.3. *Wave functions of ground states, i.e., ϕ_ℓ^g $(\ell=2,1,0,-1,-2)$ with different magnetizations $M=0$, 0.5, 1.5 (left to right) for Cases* 5–7 *(top to bottom) in Example* 4.3.

Table 4.1

The component masses $\mathcal{N}_\ell$ $(\ell=2,1,0,-1,-2)$, total masses $\mathcal{N}(\Phi^g)$, and total energies $\mathcal{E}(\Phi^g)$ of the ground states Φ^g for Cases 5–7 *(top to bottom) in Example* 4.3.

(β_1,β_2)	M	$\mathcal{N}_2$	$\mathcal{N}_1$	$\mathcal{N}_0$	$\mathcal{N}_{-1}$	$\mathcal{N}_{-2}$	$\mathcal{N}(\Phi^g)$	$\mathcal{E}(\Phi^g)$
	0	0.0627	0.2500	0.3744	0.2500	0.0627	1.0000	8.2820
$(-1,2)$	0.5	0.1530	0.3659	0.3290	0.1321	0.0199	1.0000	8.2820
	1.5	0.5865	0.3343	0.0720	0.0069	0.0002	1.0000	8.2820
	0	0.5000	0	0	0	0.5000	1.0000	8.4860
$(1,-2)$	0.5	0.6250	0	0	0	0.3750	1.0000	8.5003
	1.5	0.8750	0	0	0	0.1250	1.0000	8.6187
	0	0.3333	0	0	0.6667	0	1.0000	8.5085
$(10,2)$	0.5	0.5000	0	0	0.5000	0	1.0000	8.6309
	1.5	0.8333	0	0	0.1667	0	1.0000	9.6496

Figure 4.3 depicts the wave functions of the ground states in Cases 5–7 for magnetizations $M = 0$, 0.5, and 1.5, respectively, while Table 4.1 shows the component masses $\mathcal{N}_\ell$ $(\ell=2,1,0,-1,-2)$, total masses $\mathcal{N}(\Phi^g)$, and total energies $\mathcal{E}(\Phi^g)$ of the corresponding ground states. Figure 4.4 shows the SMA property for different (β_1,β_2,M).

From Figures 4.3–4.4, Table 4.1, and extensive numerical experiments not shown here for brevity, we observe the following: (i) When $M\in(0,2)$, for the ferromagnetic phase, $\phi_\ell^g>0$ for all $\ell=-2,-1,0,1,2$ (cf. Figure 4.3 (top row)). For the nematic phase, $\phi_2^g>0$ & $\phi_{-2}^g>0$, while $\phi_1^g=\phi_{-1}^g=\phi_0^g\equiv 0$ (cf. Figure 4.3 (middle row)).

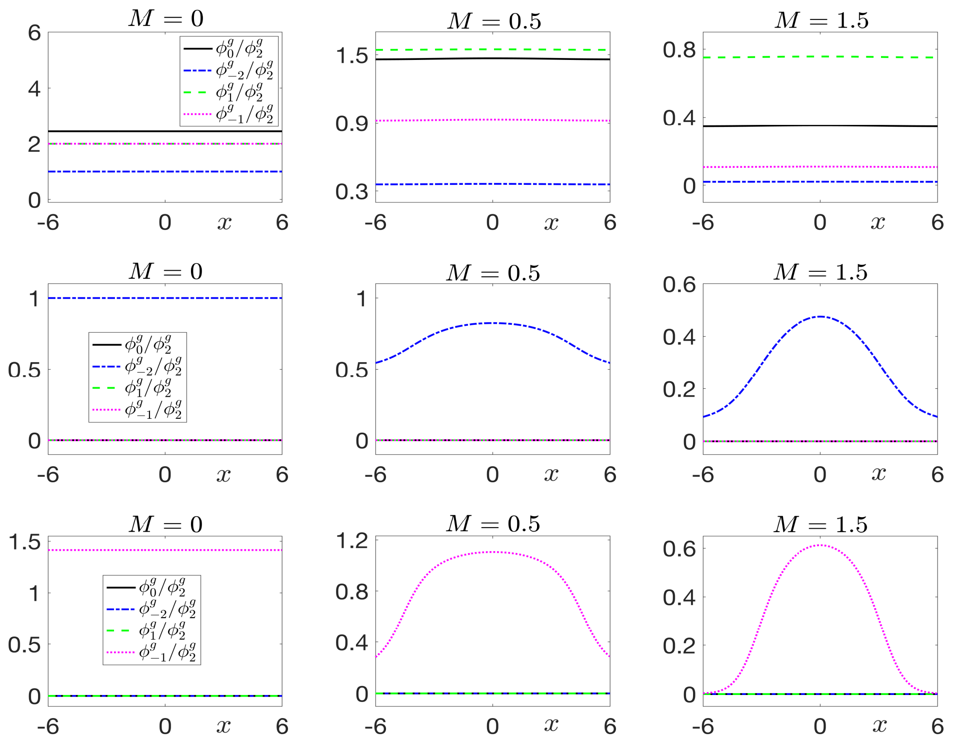

FIG. 4.4. *Plots of ϕ_1^g/ϕ_2^g (dashed line), ϕ_0^g/ϕ_2^g (solid line), ϕ_{-1}^g/ϕ_2^g (dotted line), and ϕ_{-2}^g/ϕ_2^g (dashed-dotted line) for Cases* 5–7 *(top to bottom) in Example* 4.3*, respectively, to analyze the SMA property for different parameters* (β_1, β_2, M).

For the cyclic phase, $\phi_2^g > 0$ & $\phi_{-1}^g > 0$, while $\phi_1^g = \phi_{-2}^g = \phi_0^g \equiv 0$ (cf. Figure 4.3 (bottom row)). (ii) The component masses $\mathcal{N}_\ell$ $(\ell = 2, 1, 0, -1, -2)$ of the ground state of a nonuniform spin-2 BEC system are the same as those of the corresponding spatial uniform system. Meanwhile, the total energy of the ferromagnetic ground states are independent of the magnetization M, whereas the total energy of the nematic or cyclic ground states are increased with the magnetization M (cf. Table 4.1). (iii). The SMA is valid for the ground states with the ferromagnetic phase and those with the nematic or cyclic phases as well as zero magnetization; however, it is invalid for the other cases (cf. Figure 4.4).

Example 4.4. Here we study the ground state of a two-dimensional spin-2 BEC with harmonic/box/optical lattice potentials. To this end, we take $d = 2$, $q_1 = q_2 = \pi/2$, $\eta = 0/\eta = 10$ in (4.1) for the harmonic/optical lattice potential and choose a box potential $V_{box}(\boldsymbol{x})$ as in (4.2). We consider the following three cases:

(i) Case 9. ferromagnetic phase: let $\beta_1 = -1$ & $\beta_2 = -5$.
(ii) Case 10. nematic phase: choose $\beta_1 = -1$ & $\beta_2 = -25$.
(iii) Case 11. cyclic phase: take $\beta_1 = 10$ & $\beta_2 = 2$.

Figures 4.5–4.7 show the plots of the wave functions of the ground states in Cases 9–11 with the harmonic, box, and optical lattice potential, respectively, and Table 4.2 presents the component masses $\mathcal{N}_\ell$ $(\ell = 2, 1, 0, -1, -2)$ and total energies $\mathcal{E}(\Phi^g)$ of the corresponding ground states. From these results and additional numerical experiments not shown here for brevity, one finds that our method can be applied to compute the ground state of a spin-2 BEC with general potentials. The component masses $\mathcal{N}_\ell$

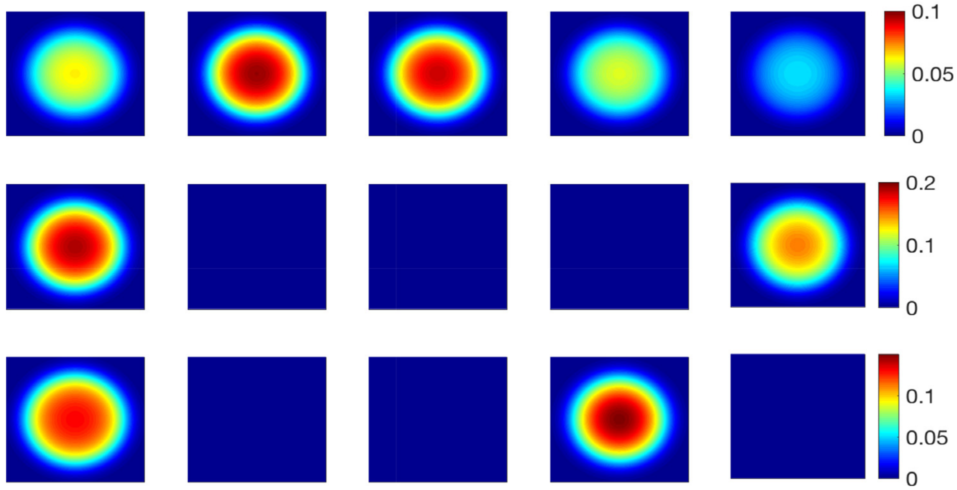

FIG. 4.5. $M = 0.5$. *Contour plots of the components of the ground states* ϕ_ℓ^g *(from left to right,* $\ell = 2, 1, 0, -1, -2$*) in Cases* 9–11 *(top to bottom) with the harmonic potential in Example* 4.4.

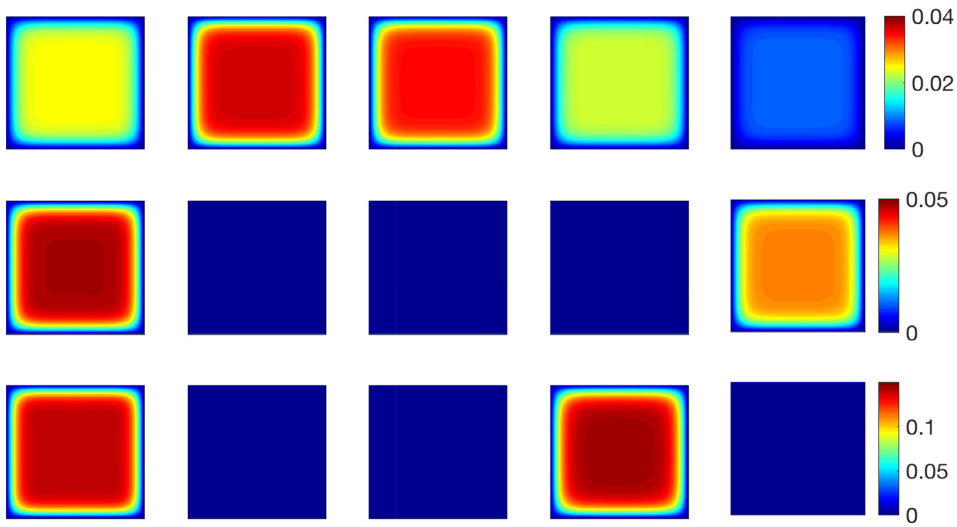

FIG. 4.6. $M = 0.5$. *Contour plots of the components of the ground states* ϕ_ℓ^g *(from left to right,* $\ell = 2, 1, 0, -1, -2$*) in Cases* 9–11 *(top to bottom) with the box potential in Example* 4.4.

are independent of the types of potentials, but the energies of the ground states are changed with different types of potentials (cf. Table 4.2). Additionally, similar to the one-dimensional case, the uniqueness, validity of SMA, and phenomena of vanishing-component of the ground state can also be concluded in the two-dimensional case.

5. Conclusion. We proposed an efficient and accurate normalized gradient flow method for computing the ground states of a spin-2 BEC by introducing three additional projection constraints, in addition to the conservation of the total mass and magnetization. A backward-forward finite difference method was applied to fully discretize the gradient flow with discrete normalization. Moreover, the ground states in a spatially uniform system, i.e., $V(\boldsymbol{x}) = 0$, were solved analytically, which give important hints to understand the properties of ground states in spatially nonuniform

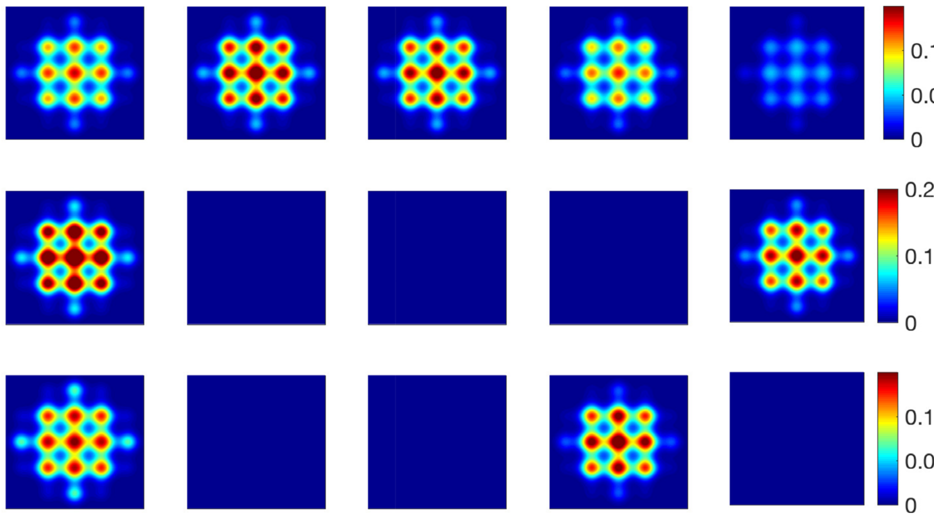

FIG. 4.7. $M = 0.5$. *Contour plots of the components of the ground states* ϕ_ℓ^g *(from left to right,* $\ell = 2, 1, 0, -1, -2$*) in Cases* 9–11 *(top to bottom) with the optical lattice potential in Example* 4.4.

TABLE 4.2
The component masses $\mathcal{N}_\ell$ *(*$\ell = 2, 1, 0, -1, -2$*) and total energies* $\mathcal{E}(\Phi^g)$ *of the ground states* Φ^g *for Cases* 9–11 *(top to bottom) in Example* 4.4.

$V(x, y)$	(β_1, β_2)	$\mathcal{N}_2$	$\mathcal{N}_1$	$\mathcal{N}_0$	$\mathcal{N}_{-1}$	$\mathcal{N}_{-2}$	$\mathcal{E}(\Phi^g)$
	$(-1, -5)$	0.1526	0.3662	0.3296	0.1318	0.0198	3.8727
$\frac{1}{2}\sum_{j=1}^{2} \nu_j^2$	$(-1, -25)$	0.6250	0	0	0	0.3750	3.8553
	$(10, 2)$	0.5000	0	0	0.5000	0	3.9848
	$(-1, -5)$	0.1526	0.3662	0.3296	0.1318	0.0198	11.7247
$\frac{\sum_{j=1}^{2}\left[\nu_j^2 + 20\sin^2\left(\frac{\pi\nu_j}{2}\right)\right]}{2}$	$(-1, -25)$	0.6250	0	0	0	0.3750	11.7012
	$(10, 2)$	0.5000	0	0	0.5000	0	11.8746
	$(-1, -5)$	0.1526	0.3662	0.3296	0.1318	0.0198	0.2024
$V_{\text{box}}(x, y)$	$(-1, -25)$	0.6250	0	0	0	0.3750	0.2009
	$(10, 2)$	0.5000	0	0	0.5000	0	0.2128

systems as well as to the choice of initial data for numerical calculations. The numerical method was then applied to study the ground states of spin-2 BECs with the ferromagnetic, nematic, and cyclic phases under harmonic, box, and optical lattice potentials in both one and two dimensions. Various numerical experiments were carried out, which suggest some interesting properties about the ground states. For example, the parameter regimes for the uniqueness, validity of SMA, and phenomena of vanishing-component were numerically partially found. Rigorous mathematical justifications for these observations are on-going.

REFERENCES

[1] A. AFTALION AND Q. DU, *Vortices in a rotating Bose-Einstein condensate: Critical angular velocities and energy diagrams in the Thomas-Fermi regime*, Phys. Rev. A, 64 (2001), 063603, https://doi.org/10.1103/PhysRevA.64.063603.

[2] M. H. ANDERSON, J. R. ENSHER, M. R. MATTHEWS, C. E. WIEMAN, AND E. A. CORNELL, *Observation of Bose-Einstein condensation in a dilute atomic vapor*, Science, 269 (1995), pp. 198–201, https://doi.org/10.1126/science.269.5221.198.

[3] X. Antoine and R. Duboscq, *Robust and efficient preconditioned Krylov spectral solvers for computing the ground states of fast rotating and strongly interacting Bose-Einstein condensates*, J. Comput. Phys., 258 (2014), pp. 509–523, https://doi.org/10.1016/j.jcp.2013.10.045.

[4] X. Antoine, A. Levitt, and Q. Tang, *Efficient spectral computation of the stationary states of rotating Bose-Einstein condensates by preconditioned nonlinear conjugate gradient methods*, J. Comput. Phys., 343 (2017), pp. 92–109, https://doi.org/10.1016/j.jcp.2017.04.040.

[5] W. Bao, *Ground states and dynamics of multicomponent Bose–Einstein condensates*, Multiscale Model. Simul., 2 (2004), pp. 210–236, https://doi.org/10.1137/030600209.

[6] W. Bao and Y. Cai, *Mathematical theory and numerical methods for Bose-Einstein condensation*, Kinet. Relat. Models, 6 (2013), pp. 1–135, https://doi.org/10.3934/krm.2013.6.1.

[7] W. Bao and Y. Cai, *Mathematical models and numerical methods for spinor Bose-Einstein condensates*, Commun. Comput. Phys., 24 (2018), pp. 899–965, https://doi.org/10.4208/cicp.2018.hh80.14.

[8] W. Bao and M. Chai, *A uniformly convergent numerical method for singularly perturbed nonlinear eigenvalue problems*, Commun. Comput. Phys., 4 (2008), pp. 135–160.

[9] W. Bao, I.-L. Chern, and F. Lim, *Efficient and spectrally accurate numerical methods for computing ground and first excited states in Bose-Einstein condensates*, J. Comput. Phys., 219 (2006), pp. 836–854, https://doi.org/10.1016/j.jcp.2006.04.019.

[10] W. Bao, I.-L. Chern, and Y. Zhang, *Efficient methods for computing ground states of spin-1 Bose-Einstein condensates based on their characterizations*, J. Comput. Phys., 253 (2013), pp. 189–208, https://doi.org/10.1016/j.jcp.2013.06.036.

[11] W. Bao and Q. Du, *Computing the ground state solution of Bose–Einstein condensates by a normalized gradient flow*, SIAM J. Sci. Comput., 25 (2004), pp. 1674–1697, https://doi.org/10.1137/S1064827503422956.

[12] W. Bao, D. Jaksch, and P. A. Markowich, *Numerical solution of the Gross-Pitaevskii equation for Bose-Einstein condensation*, J. Comput. Phys., 187 (2003), pp. 318–342, https://doi.org/10.1016/S0021-9991(03)00102-5.

[13] W. Bao and F. Y. Lim, *Computing ground states of spin-1 Bose–Einstein condensates by the normalized gradient flow*, SIAM J. Sci. Comput., 30 (2008), pp. 1925–1948, https://doi.org/10.1137/070698488.

[14] W. Bao and W. Tang, *Ground-state solution of trapped interacting Bose-Einstein condensate by directly minimizing the energy functional*, J. Comput. Phys., 187 (2003), pp. 230–254, https://doi.org/10.1016/S0021-9991(03)00097-4.

[15] W. Bao and H. Wang, *A mass and magnetization conservative and energy-diminishing numerical method for computing ground state of spin-1 Bose–Einstein condensates*, SIAM J. Numer. Anal., 45 (2007), pp. 2177–2200, https://doi.org/10.1137/070681624.

[16] R. Barnett, S. Mukerjee, and J. E. Moore, *Vortex lattice transitions in cyclic spinor condensates*, Phys. Rev. Lett., 100 (2008), 240405, https://doi.org/10.1103/PhysRevLett.100.240405.

[17] C. C. Bradley, C. A. Sackett, J. J. Tollett, and R. G. Hulet, *Evidence of Bose-Einstein condensation in an atomic gas with attractive interaction*, Phys. Rev. Lett., 75 (1995), pp. 1687–1690, https://doi.org/10.1103/PhysRevLett.75.1687.

[18] Y. Cai and W. Liu, *Efficient and accurate gradient flow methods for computing ground states of spinor Bose-Einstein condensates*, J. Comput. Phys., 433 (2021), 110183, https://doi.org/10.1016/j.jcp.2021.110183.

[19] S.-L. Chang, C.-S. Chien, and B.-W. Jeng, *Liapunov–Schmidt reduction and continuation for nonlinear Schrödinger equations*, SIAM J. Sci. Comput., 29 (2007), pp. 729–755, https://doi.org/10.1137/050642861.

[20] S.-L. Chang, C.-S. Chien, and B. Jeng, *Computing wave functions of nonlinear Schrödinger equations: A time independent approach*, J. Comput. Phys., 226 (2007), pp. 104–130, https://doi.org/10.1016/j.jcp.2007.03.028.

[21] M. Chang, C. Hamley, M. D. Barrett, J. A. Sauer, K. M. Fortier, W. Zhang, L. You, and M. S. Chapman, *Observation of spinor dynamics in optically trapped ^{87}Rb Bose-Einstein condensates*, Phys. Rev. Lett., 92 (2004), 140403, https://doi.org/10.1103/PhysRevLett.92.140403.

[22] S. Chang, W. Lin, and S. F. Shieh, *Gauss-Seidel-type methods for energy states of a multi-component Bose-Einstein condensate*, J. Comput. Phys., 202 (2005), pp. 367–390, https://doi.org/10.1016/j.jcp.2004.07.012.

[23] M. L. Chiofalo, S. Succi, and M. P. Tosi, *Ground state of trapped interacting Bose-Einstein condensates by an explicit imaginary-time algorithm*, Phys. Rev. E (3), 62 (2000), pp. 7438–7444, https://doi.org/10.1103/PhysRevE.62.7438.

[24] C. V. Ciobanu, S. K. Yip, and T. L. Ho, *Phase diagrams of F=2 spinor Bose condensates*, Phys. Rev. A, 61 (2000), 033607, https://doi.org/10.1103/PhysRevA.61.033607.

[25] I. Danaila and P. Kazemi, *A new Sobolev gradient method for direct minimization of the Gross–Pitaevskii energy with rotation*, SIAM J. Sci. Comput., 32 (2010), pp. 2447–2467, https://doi.org/10.1137/100782115.

[26] K. B. Davis, M. O. Mewes, M. R. Andrews, N. J. van Druten, D. S. Durfee, D. M. Kurn, and W. Ketterle, *Bose-Einstein condensation in a gas of sodium atoms*, Phys. Rev. Lett., 75 (1995), pp. 3969–3973, https://doi.org/10.1103/PhysRevLett.75.3969.

[27] A. Görlitz, T. L. Gustavson, A. E. Leanhardt, R. Löw, A. P. Chikkatur, S. Gupta, S. Inouye, D. E. Pritchard, and W. Ketterle, *Sodium Bose-Einstein condensates in the F=2 state in a large-volume optical trap*, Phys. Rev. Lett., 90 (2003), 090401, https://doi.org/10.1103/PhysRevLett.90.090401.

[28] T. Isoshima, M. Okano, H. Yasuda, K. Kasa, J. A. M. Huhtamäki, M. Kumakura, and Y. Takahashi, *Spontaneous splitting of a quadruply charged vortex*, Phys. Rev. Lett., 99 (2007), 200403, https://doi.org/10.1103/PhysRevLett.99.200403.

[29] Y. Kawaguchi and M. Ueda, *Spinor Bose-Einstein condensates*, Phys. Rep., 520 (2012), pp. 253–381, https://doi.org/10.1016/j.physrep.2012.07.005.

[30] M. Koashi and M. Ueda, *Exact eigenstates and magnetic response of spin-1 and spin-2 Bose-Einstein condensates*, Phys. Rev. Lett., 84 (2000), pp. 1066–1069, https://doi.org/10.1103/PhysRevLett.84.1066.

[31] T. Kuwamoto, K. Araki, T. Eno, and T. Hirano, *Magnetic field dependence of the dynamics of ^{87}Rb spin-2 Bose-Einstein condensates*, Phys. Rev. A, 69 (2004), 063604, https://doi.org/10.1103/PhysRevA.69.063604.

[32] L. Lin and I.-L. Chern, *A kinetic energy reduction technique and characterizations of the ground states of spin-1 Bose-Einstein condensates*, Discrete Contin. Dyn. Syst. Ser. B, 19 (2014), pp. 1119–1128, https://doi.org/10.3934/dcdsb.2014.19.1119.

[33] W. Liu and Y. Cai, *Normalized gradient flow with Lagrange multiplier for computing ground states of Bose–Einstein condensates*, SIAM J. Sci. Comput., 43 (2021), pp. B219–B242, https://doi.org/10.1137/20M1328002.

[34] B. Pasquiou, E. Maréchal, G. Bismut, P. Pedri, L. Vernac, O. Gorceix, and B. Laburthe-Tolra, *Spontaneous demagnetization of a dipolar spinor Bose gas in an ultralow magnetic field*, Phys. Rev. Lett., 106 (2011), 255303, https://doi.org/10.1103/PhysRevLett.106.255303.

[35] L. Simon, *Asymptotics for a class of nonlinear evolution equations, with applications to geometric problems*, Ann. of Math. (2), 118 (1983), pp. 525–571, https://doi.org/10.2307/2006981.

[36] D. M. Stamper-Kurn, M. R. Andrews, A. P. Chikkatur, S. Inouye, H. J. Miesner, J. Stenger, and W. Ketterle, *Optical confinement of a Bose-Einstein condensate*, Phys. Rev. Lett., 80 (1998), pp. 2027–2030, https://doi.org/10.1103/PhysRevLett.80.2027.

[37] T. Tian, Y. Cai, X. Wu, and Z. Wen, *Ground states of spin-F Bose–Einstein condensates*, SIAM J. Sci. Comput., 42 (2020), pp. B983–B1013, https://doi.org/10.1137/19M1271117.

[38] H. Wang, *A projection gradient method for computing ground state of spin-2 Bose-Einstein condensates*, J. Comput. Phys., 274 (2014), pp. 473–488, https://doi.org/10.1016/j.jcp.2014.06.015.

[39] A. Widera, F. Gerbier, S. Fölling, T. Gericke, O. Mandel, and I. Bloch, *Precision measurement of spin-dependent interaction strengths for spin-1 and spin-2 ^{87}Rb atoms*, New J. Phy., 8 (2006), 152, https://doi.org/10.1088/1367-2630/8/8/152.

[40] X. Wu, Z. Wen, and W. Bao, *A regularized Newton method for computing ground states of Bose-Einstein condensates*, J. Sci. Comput, 73 (2017), pp. 303–329, https://doi.org/10.1007/s10915-017-0412-0.

[41] L. Xia, X. Xu, F. Yang, W. Xiong, J. Li, Q. Ma, X. Zhou, H. Guo, and X. Chen, *Manipulation of the quantum state by Majorana transition in spinor Bose-Einstein condensates*, Phys. Rev. A, 77 (2008), 043622, https://doi.org/10.1103/PhysRevA.77.043622.

[42] Z. Yu and Z. Jiao, *Tunnelling effect of the spin-2 Bose condensate driven by external magnetic fields*, Phys. Lett. A, 320 (2004), pp. 318–321, https://doi.org/10.1016/j.physleta.2003.11.031.

[43] Y. Yuan, Z. Xu, Q. Tang, and H. Wang, *The numerical study of the ground states of spin-1 Bose-Einstein condensates with spin-orbit-coupling*, E. Asian J. Appl. Math., 8 (2018), pp. 598–610, https://doi.org/10.4208/eajam.300418.300618.

[44] W. Zhang and L. You, *An effective quasi-one-dimensional description of a spin-1 atomic condensate*, Phys. Rev. A, 71 (2005), 025603, https://doi.org/10.1103/PhysRevA.71.025603.

[45] W. Zhang, S. Yi, and L. You, *Mean field ground state of a spin-1 condensate in a magnetic field*, New J. Phys., 5 (2003), pp. 77–89, https://doi.org/10.1088/1367-2630/5/1/377.